

UNIVERSITI PUTRA MALAYSIA

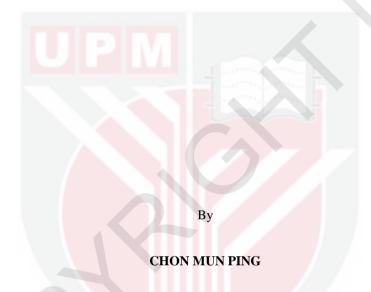
SYNTHESIS, CHARACTERISATION AND ELECTRICAL PROPERTIES OF PYROCHLORE MATERIALS IN Bi2O3-CuO-M2O5 (M = Ta AND Nb) TERNARY SYSTEMS

CHON MUN PING

FS 2015 70



SYNTHESIS, CHARACTERISATION AND ELECTRICAL PROPERTIES OF PYROCHLORE MATERIALS IN Bi_2O_3 -CuO- M_2O_5 (M = Ta AND Nb) TERNARY SYSTEMS



Thesis Submitted to the School of Graduate Studies, University Putra Malaysia, in Fulfilment of the Requirements for the Degree of Doctor of Philosophy

All material contained within the thesis, including without limitation text, logos, icons, photographs and all other artwork, is copyright material of Universiti Putra Malaysia unless otherwise stated. Use may be made of any material contained within the thesis for non-commercial purposes from the copyright holder. Commercial use of material may only be made with the express, prior, written permission of Universiti Putra Malaysia.

Copyright © Universiti Putra Malaysia



Abstract of thesis presented to the Senate of Universiti Putra Malaysia in fulfilment of the requirement for the degree of Doctor of Philosophy

SYNTHESIS, CHARACTERISATION AND ELECTRICAL PROPERTIES OF PYROCHLORE MATERIALS IN Bi_2O_3 -CuO- M_2O_5 (M = Ta AND Nb) TERNARY SYSTEMS

By

CHON MUN PING

April 2015

Chairman: Tan Kar Ban, PhD

Faculty: Science

Detailed investigations of phase diagrams and electrical properties of novel pyrochlores in the Bi_2O_3 -CuO- M_2O_5 (M = Ta and Nb) ternary systems were presented. The materials were synthesised through solid state reaction. Careful phase identification using X-ray diffraction analysis was performed to confirm the phase purities of the prepared materials and to determine the subsolidus areas in these systems. The Gibbs' phase rule approach and disappearing phase method were applied for the construction of the phase diagrams. The complete subsolidus ternary phase diagrams of the BCN and BCT systems were determined using various samples which were prepared over a wide range of temperatures, i.e. 700°C - 925°C and 700- 950°C , respectively. Phase-pure BCN pyrochlores were found to crystallise in cubic symmetry, space group Fd3m, No. 227 with lattice constants in the range of 10.4855 (5) < x < 10.5321 (3). The mechanism of this limited subsolidus series could be represented by a general formula, $Bi_{3.08-x}\text{Cu}_{1.84+2x/9}\text{Nb}_{3.08+7x/9}\text{O}_{14.16+6x/9}$ (0 \le x \le 0.36).

The cubic pyrochlore subsolidus area of BCT system could be described through two compositional variables in an overall general formula of $Bi_{2.48+y}Cu_{1.92-x}Ta_{3.6+x-y}O_{14.64+3x/2-y}$: 0.00 (1) $\leq x \leq$ 0.80 (1) and 0.00 (1) $\leq y \leq$ 0.60 (1), respectively. On the other hand, other binary phases of $Bi_7Ta_3O_{18}$, $CuTa_2O_6$ were prepared and characterised systematically for their phase formation, structural and electrical performance.

Interesting electrical properties were found in BCT cubic pyrochlores for which these materials exhibited semiconducting behaviour with recorded activation energies 0.3-0.4 eV. The dielectric constant, ϵ' of BCT material was ~75 with high dielectric losses, in the order of $10^{-2}\text{--}10^{-1}$ at room temperature and frequency of 1 MHz. A structurally related monoclinic phase $Bi_{1.92}Cu_{0.08}(Cu_{0.3}Ta_{0.7})_2O_{7.06}$ was discovered and high ϵ' , ~70 and dielectric loss were also recorded. The ac electrical conductivity of the material corresponded well to power-law frequency dependence with distinctive features of conductivity in different frequency regimes.

The cubic phase of BCN materials had a relatively lower activation energy range, 0.2-0.4 eV. Similar electrical behaviour was observed in BCN pyrochlores as to their

comparable electrical conductivities to those BCT materials. Meanwhile, the ϵ ' of BCN materials in the range of 45-70 and high dielectric losses (tan δ) of 0.04-0.12 were found.

Scanning electron microscopy was performed in order to study the surface morphologies of the prepared single phase materials. The spherulite shaped grains were randomly distributed with visible pores observed in the materials. Fourier transform infrared spectroscopy (FTIR) was used to qualitatively identify the bond stretching and bending vibration modes of the pyrochlores. Meanwhile, Raman spectroscopy was employed as a complement technique for structural analysis. Thermal analyses showed no phase transition and weight loss in BCT and BCN materials. Good stoichiometry for the prepared compositions was also confirmed using inductively coupled plasma-atomic emission spectroscopy (ICP-AES) by which a close agreement between the experimental and theoretical values were obtained, neither loss of Bi nor Cu was a problem during synthesis.

Divalent cations (M), e.g. Zn, Mg, Ni, Ca, Pb and pentavalent cations (N), e.g. Ta and Sb were chemically introduced into selected BCN and BCT materials. A complete substitutional solid solution, $Bi_{3.08}Cu_{1.84-x}Zn_xTa_{3.08}O_{14.16}$ ($0.0 \le x \le 1.84$) was obtained; however, only a narrower solid solution limit was found in the BCN system with general formula, $Bi_{2.72}Cu_{1.92-x}Zn_xNb_{3.36}O_{14.40}$ ($0.0 \le x \le 0.4$). The recorded activation energies for Zn substituted BCT pyrochlores were in the range of 0.40-1.4 eV. Extensive solid solutions were also found for the Ta replacement by Sb dopant in the BCT system. The resulted activation energies did not change significantly but remained reasonably low, i.e. in the range of 0.30-0.35 eV.

Abstrak tesis yang dikemukakan kepada Senat Universiti Putra Malaysia Sebagai memenuhi keperluan untuk ijazah Doktor Falsafah

SINTESIS, PENCIRIAN DAN SIFAT ELEKTRIK BAHAN PIROKLOR DALAM SISTEM TERNARI Bi₂O₃-CuO-M₂O₅ (M = Ta DAN Nb)

Oleh

CHON MUN PING

April 2015

Pengerusi: Tan Kar Ban, PhD

Fakulti: Sains

Penyelidikan mengenai gambar rajah fasa dan sifat elektrik dalam sistem baru ternari piroklor Bi_2O_3 -CuO- M_2O_5 (M = Ta dan Nb) telan dikaji dengan teliti. Bahan piroklor telah disintesis melalui tindak balas dalam keadaan pepejal. Data pembelauan sinar X telah digunakan untuk mengenal pasti ketulenan fasa dan untuk menentukan kawasan *subsolidus* bagi kedua-dua sistem. Gambar rajah fasa ternari bagi sistem BCT dan BCN dibina dengan menggunakan aturan fasa Gibbs' dan kaedah fasa menghilang. Sampelsampel yang disintesis dalam julat suhu antara 700°C-925°C dan 700-950°C telah digunakan untuk melengkapkan gambar rajah fasa sistem ternari *subsolidus* BCN dan BCT. Piroklor BCN fasa tulen menghablur dalam simetri kubik, kumpulan ruang Fd3m, No. 227 dengan pemalar kekisi dalam lingkungan 10.4855 (5) < x < 10.5321 (3). Mekanisme untuk siri *subsolidus* yang terhad ini boleh diwakilkan dengan formula am $Bi_{3.08-x}$ Cu_{1.84+2x9}Nb_{3.08+7x9}O_{14.16+6x9} (0 ≤ x ≤ 0.36).

Kawasan *subsolidus* piroklor BCT dapat digambarkan melalui dua pembolehubah komposisi dengan formula am Bi_{2.48+y}Cu_{1.92-x}Ta_{3.6+x-y}O_{14.64+3x/2-y}: 0.00 (1) \leq x \leq 0.80 (1) and 0.00 (1) \leq y \leq 0.60 (1). Selain itu, fasa binari Bi₇Ta₃O₁₈, CuTa₂O₆ telah disintesis dan ciri-ciri pembentukan fasa, struktur dan sifat elektrik juga dikaji dengan sistematik.

Sifat elecktrik piroklor BCT menunjukkan ciri semikonduktor dengan tenaga pengaktifan antara 0.3-0.4 eV. Pemalar dielektrik bagi bahan BCT adalah ~75 dan kehilangan dielektrik yang agak tinggi, iaitu dalam lingkungan 10^{-2} - 10^{-1} pada suhu bilik dan frekuensi 1 MHz. Fasa struktur yang berkaitan dengan fasa monoklinik $Bi_{1.92}Cu_{0.08}(Cu_{0.3}Ta_{0.7})_2O_{7.06}$ telah ditemui dan mempunyai pemalar dielektrik pukal, ~70 serta kehilangan dielektrik yang tinggi. AC kekonduksian elecktrik ini berkait rapat dengan hukum kuasa yang bergantung pada frekuensi di mana kekonduksian dalam rejim frekuensi yang berbeza boleh diwakili dengan ciri-ciri tersendiri.

Fasa kubik BCN mempunyai tenaga pengaktifan yang rendah, 0.2-0.4 eV. Sifat elektrik yang ditunjukkan oleh kubik BCN adalah setanding dengan kubik piroklor BCT. Sementara itu, pemalar dielektrik, ϵ ' kubik BCN adalah dalam lingkungan 45-70 manakala bagi nilai kehilangan dielektrik yang tinggi (tan δ), 0.04-0.12 telah dicatatkan.

Mikroskopi elektron pengimbas telah digunakan untuk mengkaji morfologi permukaan untuk sampel fasa tulen. Butiran berbentuk sferulit yang berliang dapat dilihat di atas permukaan sampel. Fourier spektroskopi inframerah (FTIR) digunakan untuk mengenal pasti regangan ikatan dan mod getaran lenturan piroklor. Selain daripada itu, specktroskopi Raman juga digunakan untuk menganalisa struktur piroklor. Analisis terma untuk piroklor BCT dan BCN tidak menunjukkan sebarang peralihan fasa dan kehilangan berat sampel. Komposisi stoikiometri untuk sampel yang dikaji juga turut dianalisa dengan spektroskopi pancaran atomik plasma ganding induktif (ICP-AES). Nilai eksperimen yang diperoleh adalah setanding dengan nilai teori sampel dan menunjukkan kehilangan Bi atau Cu tidak ketara.

Kation divalen (M) seperti Zn, Mg, Ni, Ca, Pb dan kation pentavalen (N) Ta dan Sb telah didopkan ke dalam piroklor BCN dan BCT yang terpilih. Penggantian larutan pepejal yang lengkap dalam piroklor BCT Bi $_{3.08}$ Cu $_{1.84-x}$ M $_x$ Ta $_{3.08}$ O $_{14.16}$ (0.0 \leq x \leq 1.84) telah disediakan, namun larutan pepejal dalam sistem BCN dengan formula umum Bi $_{2.72}$ Cu $_{1.92-x}$ Zn $_x$ Nb $_{3.36}$ O $_{14.40}$ adalah terhad (0.0 \leq x \leq 0.4). Tenaga pengaktifan yang dicatatkan dalam piroklor yang diganti dengan Zn berada dalam lingkungan 0.40-1.4 eV. Bagi penggantian kation pentavalen Sb ke bahan BCT, had larutan pepejal yang terbentuk adalah ekstensif. Tenaga pengaktifan tidak menunjukkan perubahan yang ketara dan berada pada tahap rendah, iaitu 0.30-0.35 eV.

ACKNOWLEDGEMENTS

I am heartily thankful to my supervisor, Dr. Tan Kar Ban, whose encouragement, guidance and patience enabled me to develop an understanding of the project. I would like to extend my sincere appreciation to Professor Dr. Zulkarnain Zainal, Professor Dr. Taufiq Yap Yun Hin and Dr. Khaw Chwin Chieh for their continuous support and suggestions throughout my research work.

Special gratitude and thanks to Professor Dr. Anthony Roy West and his postdoctoral researcher Dr. Nahum Maso for their precious discussions and assistance towards accomplishing work in phase diagrams and electrical measurement for three months at the Department of Materials Science and Engineering, University of Sheffield.

I offer my enduring gratitude to UPM Chemistry Department staffs especially Miss Nurhidayu and Madam Siti Fairouz (ICP-AES), Madam Rusnani Amirudin (IR), Madam Zaidina and Madam Gina (DTA, TGA) for their technical assistance and guidance in operating the instruments. I would also like to express my gratitude to all the staffs in Electron Microscopy Unit, Institute of Bioscience, especially to Mr. Azim for his kind assistance.

I would like to thank my lab seniors, Miss Lini and Mr. Ong Poh Shing for their guidance and patience. My thanks and appreciations also go to my lab mates, Miss Tan Phei Yi, Mr. Wong Yong Chen and Mr. Chuah You Jian for their endless support. I also wish to thank some of my close friends, Mr. Mohd Khaizarul Hanafi Bin Jamal, Miss Chan Siew Ling, Mr. Lim Yee Sing, Miss Chia Chew Theng, Miss Yuen Mei Lian and Miss Yew Sook Yan for their unfailing constant care and support, which have contributed so much to my patience and confidence in dealing with the writing.

The financial support from the Ministry of Science, Technology and Innovation (MOSTI) through National Science Fellowship (NSF) scholarship and Research University Grant Scheme (RUGS) from Ministry of Higher Education, Malaysia (MOHE) are gratefully acknowledged.

Finally, special thanks are owed to my family members and friends for their continuous support and understanding throughout the years of my educations. Their love and laughter encourage me to go through all difficulties and help me fulfil my study.

I certify that a Thesis Examination Committee has met on 28^{th} April 2015 to conduct the final examination of Chon Mun Ping on her thesis entitled "Synthesis, Characterisation and Electrical Properties of Pyrochlore Materials in Bi_2O_3 -CuO- M_2O_5 (M = Ta, Nb) Ternary Systems" in accordance with the Universities and University Colleges Act 1971 and the Constitution of the Universiti Putra Malaysia [P.U. (A) 106] 15 March 1998. The Committee recommends that the student be awarded the Doctor of Philosophy.

Members of the Thesis Examination Committee were as follows:

Nor Azah binti Yusof, PhD

Professor Faculty of Science Universiti Putra Malaysia (Chairman)

Mohamed Ibrahim bin Mohamed Tahir, PhD

Senior Lecturer Faculty of Science Universiti Putra Malaysia (Internal Examiner)

Halimah binti Mohamed Kamari, PhD

Associate Professor Faculty of Science Universiti Putra Malaysia (Internal Examiner)

Xiaoding Qi, PhD

Professor National Cheng Kung University Taiwan (External Examiner)



ZULKARNAIN ZAINAL, PhD

Professor and Deputy Dean School of Graduate Studies Universiti Putra Malaysia

Date: 17 June 2015

This thesis was submitted to the Senate of Universiti Putra Malaysia and has been accepted as fulfilment of the requirement for the degree of Doctor of Philosophy. The members of the Supervisory Committee were as follows:

Tan Kar Ban, PhD

Senior Lecturer Faculty of Science Universiti Putra Malaysia (Chairman)

Zulkarnain Zainal, PhD

Professor Faculty of Science Universiti Putra Malaysia (Member)

Taufiq Yap Yun Hin, PhD

Professor Faculty of Science Universiti Putra Malaysia (Member)

Khaw Chwin Chieh, PhD

Assistant Professor
Lee Kong Chian Faculty of Engineering and Science
Universiti Tunku Abdul Rahman
(Member)

BUJANG BIN KIM HUAT, PhD

Professor and Dean School of Graduate Studies Universiti Putra Malaysia

Date: 17 June 2015

Declaration by graduate student

I hereby confirm that:

- this thesis is my original work;
- quotations, illustrations and citations have been duly referenced;
- this thesis has not been submitted previously or concurrently for any other degree at any other institutions;
- intellectual property from the thesis and copyright of thesis are fully-owned by Universiti Putra Malaysia, as according to the Universiti Putra Malaysia (Research) Rules 2012;
- written permission must be obtained from supervisor and the office of Deputy Vice-Chancellor (Research and Innovation) before thesis is published (in the form of written, printed or in electronic form) including books, journals, modules, proceedings, popular writings, seminar papers, manuscripts, posters, reports, lecture notes, learning modules or any other materials as stated in the Universiti Putra Malaysia (Research) Rules 2012;
- there is no plagiarism or data falsification/fabrication in the thesis, and scholarly integrity is upheld as according to the Universiti Putra Malaysia (Graduate Studies) Rules 2003 (Revision 2012-2013) and the Universiti Putra Malaysia (Research) Rules 2012. The thesis has undergone plagiarism detection software.

Signature:		Date:	
Name and Ma	atric No : Chon Mun	Ping (GS 24180)	

Declaration by Members of Supervisory Committee

This is to confirm that:

- the research conducted and the writing of this thesis was under our supervision;
- supervision responsibilities as stated in the Universiti Putra Malaysia (Graduate Studies) Rules 2003 (Revision 2012-2013) are adhered to.

Signature:
Name of Chairman of Supervisory Committee: Tan Kar Ban, PhD
UPW
Signature:
Name of Member of Supervisory Committee: Zulkarnain Zainal, PhD
Signature:
Name of Member of Supervisory Committee: Taufiq Yap Yun Hin, PhD
Signature:
Name of Member of Supervisory Committee: Khaw Chwin Chieh, PhD

TABLE OF CONTENTS

ABSTRACT ABSTRAK ACKNOWLEDGEMENTS APPROVAL DECLARATION LIST OF TABLES LIST OF FIGURES LIST OF SYMBOLS AND ABBREVATIONS	i iii v vi viii xiii xv
CHAPTER 1	
INTRODUCTION	
INTRODUCTION	
1.1 Electroceramics	1
1.2 Electrical Conduction	
1.3 Dielectric Materials and Type of Polarisations	2 3
1.3.1 Electronic Polarisation	4
1.3.2 Atomic/Ionic Polarisation	4
1.3.3 Dipolar/Orientational Polarisation	4
1.3.4 Space Charge Polarisation	4
1.4 Overview of Pyrochlore and Applications	5
1.5 Formation of Pyrochlore and Solid Solution	6
1.6 Problem Statement	7
1.7 Objectives	7
CHAPTER 2 LITERATURE REVIEW	
2.1 Pyrochlore Materials	8
2.2 Pyrochlore Structure	8
2.3 Bi-based Pyrochlores	12
2.3.1 Bi_2O_3 -ZnO-Nb ₂ O ₅ System (BZN)	13
2.3.2 $Bi2O3-ZnO-Ta2O5 System (BZT)$	18
2.3.3 Relevant Bismuth-Based Pyrochlore Systems	20
CHAPTER 3	
MATERIALS AND METHODS	
3.1 Synthesis of Pyrochlore Materials	24
3.1.1 Chemical Doping	24
3.2 Phase Diagram	25
3.3 Pellet Preparation	26
3.4 Samples Characterisation	26
3.4.1 X-ray Powder Diffraction Technique (XRD)	26
3.4.2 Thermal Analysis	27

3.4.4	Fourier Transform Infrared Spectroscopy (FTIR)	28
3.4.5	Raman Spectroscopy (RS)	29
3.4.6	Inductively Coupled Plasma-Atomic Emission Spectroscopy (IC	
AES)	A.G.Y. 1	29
3.4.7	AC Impedance Spectroscopy (IS)	30
3.4.7.1	General Concepts for AC Impedance Interpretation	30
CHAPTER 4	Diagragion	
RESULTS AND I	DISCUSSION	
4.1 Struc	ctural Characteristics of Pyrochlore	36
	c Pyrochlores and Subsolidus Solution in the Bi ₂ O ₃ -CuO-Nb ₂ O ₅	
(BCN) System 4.2.1		37 39
4.2.1	Phase Formation and Reaction Pathways of the BCN System	
	Ternary Subsolidus Phase Diagram of BCN System	40
4.2.3	Structural Analyses of BCN System	47
4.2.4	Electrical Properties of BCN System	52
4.3 Cubi (BCT) System	c Pyrochlores and Subsolidus Solution in the Bi ₂ O ₃ -CuO-Ta ₂ O ₅	61
4.3.1	Phase Formation and Reaction Pathway of BCT System	64
4.3.2	Ternary Subsolidus Phase Diagram of BCT System	65
4.3.3	Structural Analyses of BCT System	74
4.3.4	Electrical Properties of BCT System	85
	oclinic Zirconolite Phase, β-phase in the Bi ₂ O ₃ -CuO-Ta ₂ O ₅ Terns	
System	octime Electronic Frasc, p-phase in the Bi ₂ O ₃ -CuO-Ta ₂ O ₅ Term	ar y 94
4.4.1	Non-Stoichiometric of New β-phase in BCT System	95
4.4.2	Phase Formation and Reaction Pathways of β-Phase	98
4.4.3	Structural Analyses of β-Phase in BCT System	100
4.4.4	Electrical Properties of β-Phase in BCT System	102
	ted Binary Phases in BCT System	120
4.5.1	Copper Tantalate (CT) and Bismuth Tantalate (BT)	120
4.5.2	XRD Analysis of Copper Tantalate, CT	122
4.5.3	Structural and Thermal Analyses of CT	123
4.5.4	Electrical Properties of CT	126
4.5.5	XRD Analysis of Bismuth Tantalate, BT	131
4.5.6	Structural and Thermal Analyses of BT	134
4.5.7	Dielectric Properties of BT	137
	ed Systems	144
4.6.1	Divalent Cation Dopants in BCN System	145
4.6.1.1	Possible Mechanisms and Solid Solution Limits	145
4.6.1.2	Electrical Properties of Divalent Dopants in BCN System	150
4.6.2	Pentavalent Cation Dopant, Ta ⁵⁺ in BCN System	154
4.6.2.1	Possible Mechanism and Solid Solution Limit	154
4.6.2.2	Electrical Properties of Ta doped BCN System	156
4.6.3	Thermal Analyses of Doped BCN Materials	158
4.6.3.1	Divalent Cation Dopants	158
		100

Thermogravimetric analysis (TGA)

Differential thermal analysis (DTA)

Scanning Electron Microscopy (SEM)

27

28

28

3.4.2.1

3.4.2.2

3.4.3

4.6.3.2	Pentavalent Cation Dopant	160
4.6.4	Structural Analyses of Doped BCN Materials	161
4.6.4.1	Divalent Cation Dopants	161
4.6.4.2	Pentavalent Cation Dopant	164
4.6.5	Divalent Cation Dopants in BCT System	168
4.6.5.1	Possible Mechanism and Solid Solution Limits	168
4.6.5.2	Electrical Properties of Divalent Dopants in BCT System	172
4.6.6	Pentavalent Cation Dopant, Sb ⁵⁺ in BCT System	176
4.6.6.1	Possible Mechanism and Solid Solution Limits	176
4.6.6.2	Electrical Properties of Sb doped BCT System	178
4.6.7	Thermal Analyses of Doped BCT Materials	179
4.6.7.1	Divalent Cation Dopants	179
4.6.7.2	Pentavalent Cation Dopant	181
4.6.8	Structural Analyses of Doped BCT Materials	182
4.6.8.1	Divalent Cation Dopants	182
4.6.8.2	Pentavalent Cation Dopant	188
4.6.9	Conclusion	191
CHAPTER 5		
CONCLUSION		192
FUTURE STUDY	Y	195
REFERENCES		196
APPENDICES		207
BIODATA OF ST	TUDENT	218
LIST OF PUBLIC	CATIONS	219
STATUS CONFI	RMATION FOR THESIS AND COPYRIGHT	220

LIST OF TABLES

Tal	ple Pa	ge
2.1	Dielectric data of $(Bi_{1.92}M_{0.08})(Zn_{0.64}Nb_{1.36})O_7$ (M = Sr, Ba) in megahertz, MW and terahertz ranges (Wang <i>et al.</i> , 2006)	18
3.1	The wavelengths used and standard solutions prepared for ICP-AES chemical analysis	29
3.2	Capacitance values and their possible interpretation (Irvine et al., 1990)	32
4.1	Summary of the phase content and synthesis condition of the prepared compositions in BCN ternary system	41
4.2	$Elemental \ analysis \ of \ Bi_{3.08-x}Cu_{1.84+2x/9}Nb_{3.08+7x/9}O_{14.16+6x/9} \ (0 \leq x \leq 0.36)$	46
4.3	Summary of Raman active frequencies and species assignments of BCN materials	49
4.4	Geometrical parameters of the prepared BCN solid solutions	52
4.5	Phases present and synthesis temperatures of samples prepared in the ${\rm Bi_2O_3\text{-}CuO\text{-}Ta_2O_5}$ ternary system	66
4.6	Elemental analysis of $Bi_{2.48+y}Cu_{1.92-x}Ta_{3.6+x-y}O_{14.64+3x/2-y}$ solid solutions, $0 \le x \le 0.80, \ 0 \le y \le 0.60$	73
4.7	Summary of Raman active frequencies and species assignments	76
4.8	Geometrical parameters of the selected BCT solid solutions	85
4.9	Refined and indexed XRD diffraction planes of BCT monoclinc zirconolite	97
4.10	Elemental analysis of the prepared Bi _{1.92} Cu _{0.08} (Cu _{0.3} Ta _{0.7}) ₂ O _{7.06}	100
4.11	Geometrical parameters of CuTa _{2-2x} O _{6-5x}	124
4.12	X-ray diffraction data for Bi ₇ Ta ₃ O ₁₈ with Miller Indexes	134
4.13	ICP-AES elemental analysis of single phase Bi ₇ Ta ₃ O ₁₈	137
4.14	Stability ranges of the substituted cations for the pyrochlore structure	145
4.15	Elemental analysis of $Bi_{2.72}Cu_{1.92-x}M_xNb_{3.36}O_{14.40}$ solid solution (M = Ni, Pb, Ca, Zn)	149
4.16	Elemental analysis of $Bi_{2.72}Cu_{1.92}Nb_{3.36-x}Ta_xO_{14.40}$ solid solution	156
4.17	Elemental analysis of divalent cations doped materials, Bi _{3.08} Cu _{1.84-} "M. Ta _{3.09} O _{14.16} solid solution (M = Mg. Ni. Zn)	171



LIST OF FIGURES

Figure		Page
2.1	Pyrochlore structure $(A_2B_2O_7)$ with 6-fold coordinated B cations and 8-coordinated A cations (Subramanian <i>et al.</i> , 1983)	9
2.2	(a) 2D representations of type I and type II cubes	9
2.2	(b) Schematic pyrochlore arrangements with type I and type II cubes (Boivin <i>et al.</i> , 1998)	10
2.3	The cations' positions in the pyrochlore structure that derived from a fluorite lattice form 1/4 of the unit cell (Subramanian <i>et al.</i> , 1983)	10
2.4	Schematic diagram of the partial unit cell (1/8 unit cell) of pyrochlore structure (Christopher <i>et al.</i> , 2002)	11
2.5	Description of pyrochlore structure based on B_2O_6 and A_2O' interpenetrating networks (a) Octahedra represent [BO ₆] units that formed a three-dimensional network (b) The resulting large cavities contain the O' and A atoms and form a second cuprite-like A_2O' tetrahedral net (c) The arrows displays the non-equivalent < 111 > directions in which the two networks interpenetrate such that the A-O'-A linkages are perpendicular to the puckered six-membered rings of octahedral (hexagonal bipyramid, AO_6O_2 '), resulting in eight-fold coordination of the A cations, where 6 O anions (48f) arising from the BO ₆ octahedra and 2 O' anions, (8b) (Levin et al., 2002)	11
2.6	Two interpenetrating networks of $(B_4 \square)O_6$ and (A_4O') networks (a) B_4 tetrahedra (filled circles) with vacant site at the centre (8a site) and (48f) oxygen outside the B_4 tetrahedra (open circles) (b) Corner shared $(B_4 \square)$ tetrahedra implying the octahedral coordination of oxygen around one B atom to give the formula $(B_{4/2} \square)O_6$ (c) A_4O' tetrahedron demonstrating the central O' atom with near perfect tetrahedral angles. These tetrahedra are corner shared with formula $A_{4/2}O'$ (Subramanian <i>et al.</i> , 1983; Pannetier and Lucas, 1970)	12
3.1	Flow diagram of the sample preparation and characterisation	25
3.2	RC element that connected in parallel	31
3.3	Complex plane plot or Cole-cole plot	33
3.4	Two semicircles (bulk and grain boundary) in Cole-cole plot	33

3.3	ceramic placed in between metal electrodes (Irvine <i>et al.</i> , 1990)	34
3.6	Combined spectroscopic plots of $Bi_{1.5}ZnTa_{1.5}O_7$ at 650°C (Khaw <i>et al.</i> , 2009)	34
3.7	Arrhenius diagram for conductivity (left) and peak frequency (right) of the $Bi_3Zn_2Sb_3O_{14}$ pyrochlore phase (Nobre $\it{et~al.}$, 2002)	35
4.1	XRD diffraction patterns of samples in $Bi_{3.08-}$ $_xCu_{1.84+2x/9}Nb_{3.08+7x/9}O_{14.16+6x/9}~(0 \leq x \leq 0.36)$ solid solutions	38
4.2	Lattice constant of Bi _{3.08-x} Cu _{1.84+2x/9} Nb _{3.08+7x/9} O _{14.16+6x/9}	39
4.3	Phase evolution study of Bi _{3.08} Cu _{1.84} Nb _{3.08} O _{14.16} in the temperature range of 600°C-910°C	40
4.4	The overall subsolidus ternary phase diagram showing the phase compatibility between BCN subsolidus pyrochlore series with other related phases in the BCN ternary system	43
4.5	Expanded region of BCN solid solutions	45
4.6	TGA thermograms of $Bi_{3.08-x}Cu_{1.84+2x/9}Nb_{3.08+7x/9}O_{14.16+6x/9}$	46
4.7	DTA thermograms of $Bi_{3.08-x}Cu_{1.84+2x/9}Nb_{3.08+7x/9}O_{14.16+6x/9}$	47
4.8	IR spectra of BCN samples	48
4.9	Raman spectra of Bi _{3.08-x} Cu _{1.84+2x/9} Nb _{3.08+7x/9} O _{14.16+6x/9} solid solutions at ambient temperature	49
4.10	(a) SEM micrograph of composition $Bi_{3.08-x}Cu_{1.84+2x/9}$ $Nb_{3.08+7x/9}O_{14.16+6x/9}$ at $x=0$	50
4.10	(b) SEM micrograph of composition $Bi_{3.08-}$ $_{x}Cu_{1.84+2x/9}Nb_{3.08+7x/9}O_{14.16+6x/9}$ at $x=0.20$	50
4.10	(c) SEM micrograph of composition $Bi_{3.08}$. ${}_{x}Cu_{1.84+2x/9}Nb_{3.08+7x/9}O_{14.16+6x/9}$ at $x=0.36$	51
4.11	Comparison between crystallite size calculated by two methods and the internal strain for each composition is plotted as a function of x	52
4.12	Real admittance, Y' as a function of frequency at different temperatures (a) $x = 0$; (b) $x = 0.20$; (c) $x = 0.36$	53
A 13	Frequency dependence of 7" as a function of frequency of	5/1

	BCN pyrochlores (a) $x = 0$; (b) $x = 0.20$; (c) $x = 0.36$ at various temperatures	
4.14	(a) Arrhenius conductivity plots of BCN samples, $0 \le x \le 0.36$ extracted at each critical frequency as a function of temperature with activation energies ranging from ~0.30-0.50 eV	55
4.14	(b) Plots of critical frequency as a function of temperature	56
4.15	(a) Complex impedance plots measured at temperatures ranging from 200°C to 450°C for sample $x=0.36$ and the inset figure shows the enlargement of the depressed semicircle	57
4.15	Complex impedance plots of samples (b) $x = 0$ and (c) $x = 0.20$	57
4.16	Combined spectroscopic plots of composition $x = 0.36$ at ~ 200 °C	58
4.17	(a) Dielectric constant (b) dielectric loss of BCN samples measured at room temperature to 300°C	59
4.18	ϵ ' as a function of frequency for sample $x = 0.36$ measured at room temperature to ~300°C	60
4.19	Combined plots of real part of dielectric constants and dielectric losses for BCN materials at room temperature and 1 MHz	61
4.20	XRD diffraction patterns of Bi _{2.48+y} Cu _{1.92-x} Ta _{3.6+x-y} O _{14.64+3x/2-y} solid solution with fixed copper content	62
4.21	XRD diffraction patterns of $Bi_{2.48+y}Cu_{1.92-x}Ta_{3.6+x-y}O_{14.64+3x/2-y}$ solid solution with fixed bismuth content	63
4.22	Lattice constant vs y for $Bi_{2.48+y}Cu_{1.92-x}Ta_{3.6+x-y}O_{14.64+3x/2-y}$ solid solution at $x=0.00$	63
4.23	Lattice constant vs x for $Bi_{2.48+y}Cu_{1.92-x}Ta_{3.6+x-y}O_{14.64+3x/2-y}$ solid solution at $y=0.00$	64
4.24	Phase evolution study of $Bi_{3.08}Cu_{1.84}Ta_{3.08}O_{14.16}$	65
4.25	The overall subsolidus Bi_2O_3 -CuO- Ta_2O_5 ternary phase diagram	68
4.26	The expanded region of single phase cubic pyrochlores	70
4.27	TGA thermograms for compositions of fixed Cu content (a-	71

- d) and composition of fixed Bi content (e-h)
- 4.28 DTA thermograms of compositions with fixed copper 72 content
- 4.29 DTA thermograms of BCT compositions with fixed Bi 72 content
- 4.30 IR spectra for compositions of fixed Cu content 75
- 4.31 IR spectra for compositions of fixed Bi content 75
- 4.32 Raman spectra of Bi_{2,48+y}Cu_{1,92-x}Ta_{3,6+x-y}O_{14,64+3x/2-y} solid 76 solutions at ambient temperature
- 4.33 (a) SEM micrograph of composition x = 0.00, y = 0.48
- 4.33 (b) SEM micrograph of composition x = 0.00, y = 0.32 78
- 4.33 (c) SEM micrograph of composition x = 0.00, y = 0.16 78
- 4.33 (d) SEM micrograph of composition x = 0.00, y = 0.00 79
- 4.33 (e) SEM micrograph of composition x = 0.24, y = 0.00 79
- 4.33 (f) SEM micrograph of composition x = 0.40, y = 0.00 80
- 4.33 (g) SEM micrograph of composition x = 0.48, y = 0.00 80
- 4.33 (h) SEM micrograph of composition x = 0.56, y = 0.00 81
- 4.33 (i) SEM micrograph of composition x = 0.72, y = 0.00 81
- 4.33 (j) SEM micrograph of composition x = 0.80, y = 0.00 82
- 4.33 (k) SEM micrograph of composition x = 0.24, y = 0.16 82
- 4.33 (1) SEM micrograph of composition x = 0.40, y = 0.08 83
- 4.34 Comparison between crystallite size calculated by two methods and the internal strain for each composition is plotted as a function of y at x = 0.00 (constant Cu content)
- 4.35 Comparison between crystallite size calculated by two methods and the internal strain for each composition is plotted as a function of x at y = 0.00 (constant Bi content)
- 4.36 (a) Arrhenius conductivity plot of samples $Bi_{2.48+y}Cu_{1.92-}$ 86 $_xTa_{3.6+x-y}O_{14.64+3x/2-y}$ at fixed Cu content (x = 0)
- 4.36 (b) Arrhenius conductivity plot of samples $Bi_{2.48+y}Cu_{1.92-}$ 86

	$_{x}Ta_{3.6+x-y}O_{14.64+3x/2-y}$ at fixed Bi content (y = 0)	
4.37	Real admittance, Y' as a function of frequency for end member composition $x=0,y=0$	87
4.38	(a) Complex impedance plot measured at room temperature	88
4.38	(b) Complex impedance plot measured at 450°C showing an inductive effect	88
4.39	Imaginary part of impedance, -Z'' as a function of frequency for composition $x=0,\ y=0$ measured at different temperatures	89
4.40	Combined spectroscopic plots of the end member composition measured at room temperature	90
4.41	(a) ε' as a function of frequency and the inset figure shows ε' as a function of temperature, (°C) measured at room temperature to ~300°C for end member composition	91
4.41	(b) $\tan \delta$ as a function of frequency and inset figure shows temperature dependence of dielectric loss, $\tan \delta$ at several frequencies for end member composition	92
4.42	(a) Combined plots of real part of dielectric constants and dielectric losses for compositions of fixed copper content (x = 0) at room temperature and 1 MHz	93
4.42	(b) Combined plots of real part of dielectric constants and dielectric losses for compositions of fixed bismuth content (y = 0) at room temperature and 1 MHz	93
4.43	Schematic presentation of the expanded zirconolite region with different mol % of Bi ₂ O ₃ , CuO and Ta ₂ O ₅ . Markers shown in the diagram are corresponded to mixture of two phases (open triangle), three phases (open circle) and zirconolite-like phase (closed symbol)	96
4.44	Indexed X-ray diffraction peaks of $\mathrm{Bi}_{1.92}\mathrm{Cu}_{0.08}(\mathrm{Cu}_{0.3}\mathrm{Ta}_{0.7})_2\mathrm{O}_{7.06}$ that crystallised in monoclinic structure, space group $C2/c$	96
4.45	Room temperature recorded X-ray diffraction patterns of BCT monoclinic zirconolite at various firing temperatures	99
4.46	DTA and TGA thermograms of BCT β -phase	100
4.47	IR spectrum of BCT β-phase	101
4.48	Surface morphology of the monoclinic zirconolite after	102

sintering for 24 h at 900°C

4.49	Real admittance, Y' as a function of frequency: (a) 100-200 K and (b) 220-576 K	104
4.49	Real admittance, Y' as a function of frequency: (c) 624-874 K with inductive effect of Y' and (d) graphical representation of typical frequency dependence ac conductivity in three regimes: (I) low-frequency (dc) plateau regime; (II) dispersive regime and (III) high-frequency plateau regime	105
4.50	Imaginary part of complex impedance, Z " at different temperatures: (a) 100-190 K; (b) 200-290 K and ~300-580 K (inset of figure) as a function of frequency	107
4.51	Plots of critical frequency as a function of temperature (a) 90-280 K and (b) 250-624 K	109
4.52	Verification of the transport property, n using plots of conductivity as a function of critical frequency (a) 90-280 K and (b) 250-624 K	110
4.53	Plots of the extracted conductivity value (from Figure 4.49) at each critical frequency as a fucntion of temprature (a) 90-280 K and (b) 250-624 K	111
4.54	Complex impedance plots measured at (a) temperature of 304 K and (b) temperature of 774 K showing additional one inductive component connected in series to existing two parallel RC elements	113
4.55	$\begin{array}{ccc} Combined & spectroscopic & plots \\ Bi_{1,92}Cu_{0.08}(Cu_{0.3}Ta_{0.7})_2O_{7.06} \text{ at temperature of 304 K} \end{array} of$	114
4.56	Dielectric constant, ϵ ' as a function of frequency measured at (a) subambient temperatures and (b) high temperatures	115
4.57	Dielectric constant, ϵ ' as a function of temperature at several fixed frequencies (a) ϵ 'at subambient temperatures with the enlarged scale as shown in the inset of figure and (b) ϵ ' at high temperatures above 304 K	116
4.58	Frequency dependence of dielectric loss, tan δ measured in different temperature ranges (a) subambient temperatures and (b) at high temperatures above 304 K	118
4.59	Temperature dependence of dielectric loss, tan δ at several fixed frequencies (a) subambient temperatures and (b) high temperatures above 304 K	119

4.60	XRD diffraction patterns of CuTa _{2-2x} O _{6-5x}	122
4.61	IR spectra of CuTa _{2-2x} O _{6-5x}	123
4.62	(a) SEM micrograph of CuTa _{1.8} O _{5.5}	124
4.62	(b) SEM micrograph of CuTa _{1.6} O ₅	124
4.63	(a) DTA thermograms of $CuTa_{2-2x}O_{6-5x}$	125
4.63	(b) TGA thermograms of CuTa _{2-2x} O _{6-5x}	125
4.64	Cole-Cole plot of CuTa _{1.8} O _{5.5} at ~100°C	126
4.65	M" plot showing distorted semicircle for sample $x = 0.1$	127
4.66	Combined spectroscopic plots of CuTa _{1.8} O _{5.5} at 100°C	127
4.67	Admittance plot, Y' of $CuTa_{2-2x}O_{6-5x}$ at 1-10 kHz (Open symbol: $x = 0.2$; Closed symbol: $x = 0.1$)	128
4.68	Arrhenius conductivity plots for samples $CuTa_{1.8}O_{5.5}$ and $CuTa_{1.6}O_5$, respectively	129
4.69	ε ' of $x = 0.1$ as a function of temperature and frequency (inset figure)	130
4.70	$tan \ \delta \ for \ x = 0.1 \ as \ a \ function \ of \ temperature \ and \ frequency \ (inset \ figure)$	131
4.71	X-ray diffraction patterns for phase evolution of Bi ₇ Ta ₃ O ₁₈ at different annealing temperatures	132
4.72	Refined and indexed X-ray diffraction pattern of prepared single phase Bi ₇ Ta ₃ O ₁₈	133
4.73	FTIR spectrum of $Bi_7Ta_3O_{18}$ recorded at wave number of $1000\text{-}250~\text{cm}^{\text{-}1}$	135
4.74	SEM image of Bi ₇ Ta ₃ O ₁₈ captured at 3k magnification	136
4.75	DTA and TGA thermograms of single phase $Bi_7Ta_3O_{18}$	136
4.76	Complex Cole–Cole plots of Bi ₇ Ta ₃ O ₁₈ at different temperatures and incomplete arcs at temperatures above 500°C are shown in the inset of figure	137
4.77	Combined spectroscopic plots of M" and -Z" as a function of frequency at temperature of 352°C	138
4.78	Real admittance plots, Y' as a function of frequency at	139

various temperatures for Bi₇Ta₃O₁₈

4.79	Arrhenius conductivity plot of $Bi_7Ta_3O_{18}$ with activation energy, $E_a \sim 0.97 \ ev$	139
4.80	Imaginary part of electric modulus plots, M" as a function of frequency at various temperatures for $Bi_7Ta_3O_{18}$	140
4.81	Imaginary part of impedance plots, -Z" as a function of frequency at different temperatures for $Bi_7Ta_3O_{18}$	141
4.82	Arrhenius plot of the peak frequency extracted from the plots of imaginary impedance, Z'' as a function of temperature	142
4.83	Real part of permittivity plots, ε' as a function of temperature at various frequencies	143
4.84	Dielectric loss, $\tan \delta$ measured over a wide range of temperatures at different frequencies	144
4.85	XRD patterns of Ca doped BCN materials, $(Bi_{2.72}Cu_{1.28-x}Ca_x)(Cu_{0.64}Nb_{3.36})O_{14.40}$ solid solution	146
4.86	XRD patterns of Pb doped BCN materials, (Bi _{2.72} Cu _{1.28-x} Pb _x)(Cu _{0.64} Nb _{3.36})O _{14.40} solid solution	147
4.87	XRD patterns of Ni doped BCN materials, (Bi _{2.72} Cu _{1.28})(Cu _{0.64-x} Ni _x Nb _{3.36})O _{14.40} solid solution	147
4.88	$\begin{array}{cccccccccccccccccccccccccccccccccccc$	148
4.89	Lattice constants of BCN pyrochlores doped with various divalent cations, $Bi_{2.72}Cu_{1.92-x}M_xNb_{3.36}O_{14.40}$ solid solution (M = Zn, Ca, Pb, Ni)	148
4.90	Arrhenius conductivity plots of divalent cations doped materials, $Bi_{2.72}Cu_{1.92-x}M_xNb_{3.36}O_{14.40}$ at $x=0.1$ (M = Zn, Ca, Pb, Ni)	151
4.91	Arrhenius conductivity plots of Zn doped materials, $Bi_{2.72}Cu_{1.92\text{-}x}Zn_xNb_{3.36}O_{14.40}$	151
4.92	Real part of (a) dielectric constant and (b) dielectric loss vs concentration of various divalent cations in doped BCN materials, $\mathrm{Bi}_{2.72}\mathrm{Cu}_{1.92\text{-x}}\mathrm{M_xNb}_{3.36}\mathrm{O}_{14.40}(M=\mathrm{Ca,Pb,Ni,Zn})$ at room temperature and 1 MHz	153
4.93	XRD patterns of the complete Bi _{2.72} Cu _{1.92} Nb _{3.36-x} Ta _x O _{14.40} solid solution	155

4.94	Lattice constants vs x value of the complete solid solution of Ta doped BCN materials, $Bi_{2.72}Cu_{1.92}Nb_{3.36-x}Ta_xO_{14.40}$	155
4.95	Arrhenius conductivity plots of $Bi_{2.72}Cu_{1.92}Nb_{3.36\text{-x}}Ta_xO_{14.40}$ solid solution	157
4.96	ϵ' and tan δ measured at room temperature as a function of composition $0 \leq x \leq 3.36$ for $Bi_{2.72}Cu_{1.92}Nb_{3.36\text{-}x}Ta_xO_{14.40}$ solid solution	158
4.97	TGA thermograms of selected divalent cations doped in BCN materials	159
4.98	DTA thermograms of selected doped materials (a) $Bi_{2.72}Cu_{1.82}Pb_{0.1}Nb_{3.36}O_{14.40}$; (b) $Bi_{2.72}Cu_{1.82}Ca_{0.1}Nb_{3.36}O_{14.40}$; (c) $Bi_{2.72}Cu_{1.72}Ni_{0.2}Nb_{3.36}O_{14.40}$ and (d) $Bi_{2.72}Cu_{1.52}Zn_{0.4}Nb_{3.36}O_{14.40}$	159
4.99	TGA thermograms of Ta doped in BCN materials	160
4.100	DTA thermograms of complete solid solution $Bi_{2.72}Cu_{1.92}Nb_{3.36-x}Ta_xO_{14.40}$	160
4.101	IR spectra of selected samples of divalent cations doped in BCN materials	161
4.102	SEM micrograph of Bi _{2.72} Cu _{1.82} Ca _{0.1} Nb _{3.36} O _{14.40}	162
4.103	SEM micrograph of Bi _{2.72} Cu _{1.82} Pb _{0.1} Nb _{3.36} O _{14.40}	162
4.104	SEM micrograph of Bi _{2.72} Cu _{1.82} Ni _{0.1} Nb _{3.36} O _{14.40}	163
4.105	SEM micrograph of Bi _{2.72} Cu _{1.72} Ni _{0.2} Nb _{3.36} O _{14.40}	163
4.106	SEM micrograph of $Bi_{2.72}Cu_{1.52}Zn_{0.4}Nb_{3.36}O_{14.40}$	164
4.107	IR spectra of complete solid solution $Bi_{2.72}Cu_{1.92}Nb_{3.36-x}Ta_xO_{14.40}$	165
4.108	SEM micrograph of $Bi_{2.72}Cu_{1.92}Nb_{2.86}Ta_{0.5}O_{14.40}$	166
4.109	SEM micrograph of $Bi_{2.72}Cu_{1.92}Nb_{2.24}Ta_{1.12}O_{14.40}$	166
4.110	SEM micrograph of $Bi_{2.72}Cu_{1.92}Nb_{1.12}Ta_{2.24}O_{14.40}$	167
4.111	SEM micrograph of $Bi_{2.72}Cu_{1.92}Ta_{3.36}O_{14.40}$	167
4.112	XRD patterns of $Bi_{3.08}Cu_{1.84-x}Mg_xTa_{3.08}O_{14.16}$ solid solution	169

4.113	XRD patterns of Bi _{3.08} Cu _{1.84-x} Ni _x Ta _{3.08} O _{14.16} solid solution	169
4.114	XRD patterns of complete $Bi_{3.08}Cu_{1.84\text{-x}}Zn_xTa_{3.08}O_{14.16}$ solid solution	170
4.115	Variation of lattice constants of divalent-doped BCT pyrochlores	170
4.116	Arrhenius conductivity plots of $Bi_{3.08}Cu_{1.84-x}M_xTa_{3.08}O_{14.16}$ solid solution (M = Mg, Ni)	173
4.117	Arrhenius conductivity plots of $Bi_{3.08}Cu_{1.84-x}Zn_xTa_{3.08}O_{14.16}$ with activation energies ranging from $0.35~eV$ - $1.40~eV$	173
4.118	(a) Real part of dielectric constant vs x values of divalent cations doped in BCT materials, $Bi_{3.08}Cu_{1.84-x}M_xTa_{3.08}O_{14.16}$ (M = Mg, Ni)	174
4.118	(b) Dielectric loss vs x values of divalent cations doped in BCT materials, $Bi_{3.08}Cu_{1.84-x}M_xTa_{3.08}O_{14.16}$ (M = Mg, Ni)	175
4.119	ϵ ' and $\tan \delta$ as a function of composition $0 \le x \le 1.84$ measured at room temperature for $Bi_{3.08}Cu_{1.84}$. $_xZn_xTa_{3.08}O_{14.16}$ solid solution	175
4.120	XRD patterns of Bi _{3.08} Cu _{1.84} Ta _{3.08-x} Sb _x O _{14.16} solid solution	176
4.121	Variations of lattice constant with respect to Sb content	177
4.122	Arrhenius conductivity plots of Bi _{3.08} Cu _{1.84} Ta _{3.08-x} Sb _x O _{14.16} solid solution	178
4.123	ϵ' and tan δ as a function of composition of $Bi_{3.08}Cu_{1.84}Ta_{3.08}.$ $_xSb_xO_{14.16}$ solid solution	179
4.124	TGA thermograms of selected divalent cations doped in BCT materials	180
4.125	DTA thermograms of selected samples (a) $Bi_{3.08}Cu_{1.64}Mg_{0.2}Ta_{3.08}O_{14.16}$ (b) $Bi_{3.08}Cu_{1.64}Ni_{0.2}Ta_{3.08}O_{14.16}$ (c) $Bi_{3.08}Cu_{1.44}Zn_{0.4}Ta_{3.08}O_{14.16}$ d) $Bi_{3.08}Cu_{1.2}Zn_{0.64}Ta_{3.08}O_{14.16}$ e) $Bi_{3.08}Cu_{0.6}Zn_{1.24}Ta_{3.08}O_{14.16}$ f) $Bi_{3.08}Zn_{1.84}Ta_{3.08}O_{14.16}$	180
4.126	TGA thermograms of Sb doped BCT materials	181
4.127	DTA thermograms of pentavalent cation doped in BCT materials	182

4.128	IR spectra of selected samples of divalent cations doped in BCT materials	183
4.129	SEM micrograph of $Bi_{3.08}Cu_{1.64}Mg_{0.2}Ta_{3.08}O_{14.16}$	184
4.130	SEM micrograph of $Bi_{3.08}Cu_{1.64}Ni_{0.2}Ta_{3.08}O_{14.16}$	184
4.131	SEM micrograph of $Bi_{3.08}Cu_{1.44}Zn_{0.4}Ta_{3.08}O_{14.16}$	185
4.132	SEM micrograph of Bi _{3.08} Cu _{1.2} Zn _{0.64} Ta _{3.08} O _{14.16}	185
4.133	SEM micrograph of Bi _{3.08} Cu _{0.84} ZnTa _{3.08} O _{14.16}	186
4.134	SEM micrograph of Bi _{3.08} Cu _{0.6} Zn _{1.24} Ta _{3.08} O _{14.16}	186
4.135	SEM micrograph of Bi _{3.08} Cu _{0.2} Zn _{1.64} Ta _{3.08} O _{14.16}	187
4.136	SEM micrograph of Bi _{3.08} Zn _{1.84} Ta _{3.08} O _{14.16}	187
4.137	IR spectra of Sb doped BCT materials	188
4.138	SEM micrograph of Bi _{3.08} Cu _{1.84} Ta _{2.58} Sb _{0.5} O _{14.16}	189
4.139	SEM micrograph of Bi _{3.08} Cu _{1.84} Ta ₂ Sb _{1.08} O _{14.16}	189
4.140	SEM micrograph of Bi _{3.08} Cu _{1.84} Ta _{1.58} Sb _{1.5} O _{14.16}	190
4.141	SEM micrograph of Bi _{3.08} Cu _{1.84} TaSb _{2.08} O _{14.16}	190

LIST OF SYMBOLS AND ABBREVATIONS

ACAlternating current **BCN** Bismuth copper niobate **BCT** Bismuth copper tantalate Bismuth magnesium niobate **BMN BMT** Bismuth magnesium tantalate

BZN Bismuth zinc niobate Bismuth zinc tantalate **BZT CSD** Chemical solution deposition **CVD** Chemical vapour deposition

Direct current dc

DTA Differential thermal analysis

Faced-centred cubic fcc

FTIR or IR Fourier transform infrared spectroscopy

FWHM/B Full width at half maximum Hexagonal tungsten bronze HTB

International Centre for Diffraction Data **ICDD** Inductively coupled plasma-atomic emission **ICP-AES**

spectroscopy

Low temperature co-fired ceramic LTCC

MHD Magnetohydrodynamic **MLCC** Multilayer ceramic capacitor **PLD** Pulsed laser deposition RS Raman spectroscopy **SEM** Scanning electron microscopy

SOFC Sold oxide fuel cells

Temperature coefficient of capacitance TCC

Thermogravimetry analysis **TGA**

WD Working distance **XRD** X-ray diffraction

Lattice constants/ angles for each symmetry $a,b,c/\alpha,\beta$

Α

Temperature dependent constant

A* or Y* Admittance

A' or Y' Real part of admittance A" or Y" Imaginary part of admittance

Bulk capacitance $C_{\rm b}$

Grain boundary capacitance C_{gb} C_{o} Vacuum capacitance D Coherent scattering length Interplanar spacing/ d-spacing d

Internal strain 3

ε* Complex permittivity

ε' Relative permittivity/ dielectric constant

Imaginary part of permittivity Permittivity of free space ϵ_{o} activation energy for conduction E_a

GF Geometrical factors h, k, l Miller indices

Imaginary component j k_B Boltzman's constant Thickness M* Complex modulus M'/M'' Real part of modulus/ Imaginary part of modulus MC Microwave ceramics Dissipation factor/ quality factor Q R_b **Bulk Resistance** R_{gb} Grain boundary Resistance T Crystallite size (Scherrer method) $tan \delta$ Dielectric loss T_{c} Critical temperature TCC Temperature coefficient of capacitance ΤCε' Temperature coefficient of permittivity Z Unit formula Z^* Complex impedance Z'/Z'' Real part of impedance/ Imaginary part of impedance Conductivity/ dc conductivity/ ac conductivity $\sigma / \sigma_0 / \sigma_{ac}$ pre-exponential factor σ_0 Impedance relaxation frequency or relaxation time τ θ Bragg angle λ Wavelength Wavenumber ν Angular frequency ω

frequency of maximum loss

 ω_{max}

CHAPTER 1

INTRODUCTION

1.1 Electroceramics

Research advancement in the field of electroceramics is driven by their technological applications. Microelectronics are the superior form of the ceramic substances whose properties and applications are found in many areas, such as power conversion and storage, communications, computation, automation, consumer products and medical industries. Electroceramics are widely applied in insulating materials, high dielectric capacitors, ultrasonic transducers, resistors, thin film capacitors and communications filters, solid oxide fuel cells (SOFC) and batteries. Therefore, their unique functional capabilities provide a wide spectrum of electrical and microelectronic devices and other related applications.

In fact, the advanced functional components are made of integrated materials which are useful in the miniaturised systems where interfaces of the materials play a crucial role. The integration of electroceramic thin films onto the substrates and the combination of bulk ceramics of different kinds or other materials such as glasses, metals or polymers are common in the evolution of multifunctional components. The objectives of electrical and electronic components miniaturisation are to produce materials with the specific properties, required shapes and sizes within the specified dimensional tolerances and at reasonable cost. Electroceramics have experienced the progression from microtechnology towards nanotechnology. The nanosize effects and the application of new characterisation techniques that reveal the nanometric scale features are therefore of the realm of research (Setter et al., 2000).

Practically, these materials are produced by conventional powder processing, tape casting or screen printing techniques and then followed by sintering processes. In the late 1980s, these techniques were progressively supplemented by thin film deposition techniques such as sputtering, pulsed laser deposition (PLD), chemical solution deposition (CSD) and the chemical vapour deposition (CVD). During the deposition processes, these materials are prepared on a microscopic scale without powder processing as an intermediate step because the synthesised temperatures are below the typical sintering temperatures of the bulk ceramics (Setter *et al.*, 2000).

Electroceramics are in general comprised of dielectrics, conductive, magnetic and optical ceramics. Examples for the dielectrics are piezo, pyro, ferroelectrics whereas the superconductors, conductors and semiconductors with both ionically and/or electronically are categorised as conductive ceramics. The primary distinction between a dielectric (or insulator) and a semiconductor lies in the difference between their energy band gap in which the latter has a smaller energy band gap and the dominant charge carriers are generated mainly by thermal excitation in the bulk under normal ranges of temperature and pressure ranges (Kwan, 2004). In dielectric, charge carriers are mainly injected from the electrical contacts or other external sources simply because the band gap of dielectric is relatively larger and therefore, higher amount of energy is required for the band-to-band transition. The occurrence of dielectric

phenomena are the interaction between the free charges with the external forces, such as electric fields, magnetic fields, electromagnetic waves, mechanical stress or temperature. For non-magnetic dielectric materials, the phenomena are encompassed by mainly electric polarisation, resonance, relaxation, energy storage, energy dissipation, thermal, mechanical, optical effects and their interrelations. In general, electroceramics offer a wide variety of functions, notably in microelectronics and communication components. The fabrication and miniaturisation of electrical and electronic devices are prevalent which had made much fascination in the research development of electroceramics.

1.2 Electrical Conduction

Electrical conduction is primarily governed by the manner of generating charge carriers in a material. The electrical conductivities of the materials are ranging from superconductors through those of metals, semiconductors and highly resistive insulators. Electrical conductivity can be divided into three different categories (Kwan, 2004) which outlined as below:

- i) Intrinsic conductivity: Charge carriers are developed in the material based on its chemical structure.
- ii) Extrinsic conductivity: Charge carriers are initiated by material impurities, which may be introduced by fabrication processes or deliberately doped into it for a distinct purpose.
- iii) Injection-controlled conductivity: Charge carriers are injected into the material mainly from metallic electrodes via a metal-material interface.

The electrical conductivity follows the empirical equation as given in Equation (1.1)

$$\sigma = \sigma_0 \exp\left(-E_\sigma/kT\right) \tag{1.1}$$

where σ_0 is the pre-exponential factor, E_{σ} is the activation energy, k is the Boltzman constant and T is the temperature in kelvin. In reality, the electrical conduction involves various transport processes and under certain condition, it may involve both ionic and electronic conductions (Kwan, 2004).

Generally, the fundamental charge carriers are the cations, anions, electrons and electron holes and the total conductivity is given as

$$\sigma = \sigma_c + \sigma_a + \sigma_n + \sigma_p \tag{1.2}$$

where σ_c , σ_a , σ_n , σ_p are the cation, anion, electron and electron hole conductivities, respectively. The individual conductivity may be written in terms of their transport numbers:

(t):
$$\sigma_c = t_c \sigma$$
, $\sigma_a = t_a \sigma$, $\sigma_n = t_n \sigma$ and $\sigma_n = t_n \sigma$ (1.3)

and the sum of the transport numbers of all the charge carriers are equivalent to unity:

$$t_c + t_a + t_n + t_p = 1$$
 (1.4)

 $t_c + t_a + t_n + t_p = 1 \qquad (1.4)$ The summation of ionic conductivity (1.5) and electronic conductivity (1.6) gives rise to the total electrical conductivity (1.7) (Manning, 1962).

$$\sigma_{\rm ion} = \sigma_{\rm c} + \sigma_{\rm a} \tag{1.5}$$

$$\sigma_{\rm el} = \sigma_{\rm n} + \sigma_{\rm p} \tag{1.6}$$

$$\sigma = \sigma_{\rm ion} + \sigma_{\rm el} \tag{1.7}$$

It is common that only one type of charge carrier prevails the charge transport and the contribution from minority carriers is insignificant. The mobilities of electrons and electron holes in oxides are generally several orders of magnitude (~10⁴-10⁸) greater than those of the ions. In some cases, the oxide may still be essentially an electronic conductor though the concentration of electron or electrons holes is lower than that of the ionic charge carriers. The relative importance of ionic and electronic conductivities will always vary incredibly with temperature and oxygen partial pressure (Manning, 1962).

In fact, most metal oxides are electronic conductors at elevated temperatures. The conductivities of these oxides increase with increasing temperature and the reason is due to the increase of the number of electronic defects with temperature. Transition metal monoxides are metallic conductors for which their conductivities decrease with increasing temperature as the mobility of electronic defects decrease with increasing temperature. For certain oxides, e.g. p-conducting acceptor-doped perovskites demonstrate metallic-like conductivity in which the conductivity decreases with temperature and the depreciation of conductivity is attributed to decreased number of electron holes with increasing temperature, thus the conductivity cannot be classified as metallic (Manning, 1962).

The electronic conductivity, σ_{el} of a semiconducting oxide is given in Equation (1.6). As mentioned earlier, one type of charge carrier will usually dominate and in some cases where an oxide is close to stoichiometric, both n- and p-typed conductivity may contribute significantly to the electronic conductivity.

1.3 **Dielectric Materials and Type of Polarisations**

The important electrical property of dielectric materials is relative permittivity (ϵ), which is also known as dielectric constant. It relies greatly on the frequency of the alternating electric field or the rate of the change of the time-varying field. Likewise, the chemical structure and the imperfections such as defects of the materials, as well as some other physical parameters including temperature and pressure play a significant role in determining the dielectric properties (West, 1999). A dielectric material is made up of atoms or molecules that possess one or more basic types of electric polarisation, including electronic, atomic (or ionic), dipolar and interface/space charge polarisations. The application of an electric field causes the formation and movement of dipoles is called polarisation. When an electric field is applied to the material, dipoles within the atomic or molecular structure are induced and aligned with the direction of that applied

field. Any permanent dipoles that are previously present in the material are also aligned with that particular field. In this case, the material is said to be polarised. The degree of the overall polarisation is affected by the time variation of the electric field as each type of the polarisation requires time to perform.

1.3.1 Electronic Polarisation

It is always present in atoms or molecules in all kinds of materials. When the atom is located in an electric field, the charged particles experience an electric force as a result of which the centre of the negative charge cloud is displaced with respect to the nucleus. A dipole moment is induced by electric field and the atom is said to be electronically polarised (Raju, 2003).

1.3.2 Atomic/Ionic Polarisation

It is sometimes referred as vibrational polarisation due to the distortion of the normal lattice vibration and the electric field causes the atoms or ions of a polyatomic molecule to be displaced relative to each other. In other words, this is the displacement of positive ions with respect to negative ions and the induced dipole moment is slightly dependent on temperature (Kwan, 2004).

1.3.3 Dipolar/Orientational Polarisation

This polarisation is different from the electronic and ionic polarisations in which it can occur even when an external electric field is not applied and this happens only in materials consisting of molecules or particles with a permanent dipole moment. The electric field causes the reorientation of the dipoles toward the direction of the field. When an electric field is applied to a polar dielectric, the following steps will take place:

- i) The distance between the centres of the negative and positive electric charges increases slightly and the dipole moment becomes greater due to the action of electric field because the dipole experiences tension.
- ii) The dipoles turn so that the positively charged end faces the negative electrode and the negatively charged end faces the positively electrode. The sum of the individual dipole moments will now not be equal to zero (Rajput, 2004).

1.3.4 Space Charge Polarisation

The space charge or translational polarisation is observed in materials containing intrinsic free charges such as ions, holes or electrons. This polarisation is caused by the accumulation of charges at the multiphase of dielectrics. When one of the phases has a higher resistivity than the other, the charge moves on the surface when the material is placed in an electric field. This usually found in ferrites and semiconductors at elevated temperatures (Raju, 2003).

1.4 Overview of Pyrochlore and Applications

Oxides are the biggest family of solid state materials. Different types of oxides emerge from a wide variety of structures, bonding characters and compositions and these parameters have strong correlation with their physical and electrical properties. With general knowledge on the chemical nature of different elements, the information is used to design new materials with the desired properties for many applications.

Examples of mixed metal oxides with the formula $A_2B_2O_7$ are oxide pyrochlores which show good chemical and thermal stability. Pyrochlore oxides are useful in various devices and applications due to their broad spectrum of properties such as electrical, magnetic, dielectric, optical and catalytic behaviour. These properties are generally controlled by the factors, i.e. ionic size, polarisability of the ions, electronic configuration and the preparative conditions. They could be viewed as doubled unit cells of derivative fluorite structure, AO_2 for which the cationic sites are differentiated into both A and B sites. As a consequence, hundreds of different compositions of pyrochlores with various properties could be yielded. Pyrochlore structure has great tolerance towards vacancies and therefore, defect pyrochlores with vacancies in A and/or O sites can attribute to many compounds in this family.

Pyrochlore materials can be used as solid electrolytes, oxygen electrodes, catalysts as well as in the active and passive electronic components e.g. high permittivity microwave filters, thermistors, gas sensor, switching elements and thick film resistors (Boivin *et al.*, 1998). Stoichiometric oxide pyrochlores containing elements in their maximum oxidation state and high ionic polarisability always exhibit good dielectric properties, e.g. Cd₂Nb₂O₇, Ln₂Ti₂O₇ are excellent ferroelectric materials. Dielectric constants are fairly large in many niobates, tantalates and titanates and these materials can be used as high permittivity ceramics (Tan *et al.*, 2005; Sreekantan *et al.*, 2008; Khaw *et al.*, 2009). Thermistors are commonly made from oxide components with spinel or related structure, e.g. Bi₂CrNbO₇ and Bi₂CrTaO₇ with the pyrochlore structures are used for temperature compensation, voltage stabilisation and current time relays. Many Pb- and Bi- containing precious metals are used to make thick film resistors with low and reproducible sheet resistance. These materials are unaffected by humidity and have negligibly small temperature coefficient of resistance (Van Loan, 1972).

Zirconate pyrochlores, e.g. $Pr_2Zr_2O_7$ doped with 10% In_2O_3 could also be the promising materials to be used as electrodes for open cycle magnetohydrodynamic (MHD) power generation schemes as they have excellent corrosion and shock resistance, good electronic and thermal conductivity (Meadowcroft, 1968). However, more experimentation and feasibility studies are required as the commercial utilisation of MHD power generation is still much in the experimental stages. On the other hand, pyrochlores materials are also applied in switching elements that show sudden and abnormally great change in electrical conductivity at a given temperature. The change in electrical conductivity can be caused by direct variation of temperature, the element by external source or by internal heating effects by the passage of current. Examples VO_2 and doped $BaTiO_3$ are both applied in switching elements for temperature sensitive electrical switches and fire extinguishers (Subramanian *et al.*, 1983).

Pyrochlores also play a crucial role in the nuclear waste disposal and the understanding of the detailed phase stability relationships enables a careful screening of additives for fixation of radioactive ions. Examples such as Ln, Zr, Mo, Ru are introduced into pyrochlore or the related crystalline phases for easy transportation, handling and disposal. Besides, pyrochlores are also used as microwave dielectrics in microwave resonators. The development of microwave dielectric materials depends strongly on the materials with high quality factor, Q (reciprocal of dielectric loss) (Q > 10,000). The recent device manufactures also emphasise on the process compatibility with low resistivity metals and allow low Q dielectrics (Q \approx 200). Ceramics in the bismuth zinc niobate (BZN) and bismuth zinc tantalate (BZT) ternary systems with pyrochlore structure are promising dielectrics because of their suitable Q values and the temperature coefficient of capacitance which can be compositionally tailor-made to a low value (Nino *et al.*, 2001; Youn *et al.*, 2002).

1.5 Formation of Pyrochlore and Solid Solution

A broad range of cations is substituted at the A and B sites of pyrochlores and this leads to hundreds of different compositions with various properties. In Bi₂O₃-ZnO-Nb₂O₅ (BZN) system, an ideal composition could be Bi₃Zn₂Nb₃O₁₄ in which it is presumed that the Zn cation is apportioned evenly at both A- and B- sites. Alternatively, the chemical formula of BZN could be written as (Bi_{1.5}Zn_{0.5})(Zn_{0.5}Nb_{1.5})O₆O'. Bismuth-based pyrochlore structure has a great tolerance for accepting different ions at the A, B and O sites and the unambiguous correlation among the ionic radii of the A and B cations is crucial in order to maintain the stability of pyrochlores. Nevertheless, the stability of the pyrochlore structure also depends on the electronegativity of the cations, charge neutrality and thermodynamic stability of the competitive phases. The combination of A and B cations should yield the same average charge in order to maintain electroneutrality. The stability range has been stipulated by the cation radii ratio R_A/R_B. The substituted cations must have appropriate ionic radii to fit into the pyrochlore structure based on the upper and lower radius limits at which these values are given as $0.87 < r_A < 1.17$, $0.58 < r_B < 0.775$ Å and $0.96 < r_A < 1.29$, $0.54 < r_B < 0.76$ Å for $A_2^{3+}B_2^{4+}O_7$ and $A_2^{2+}B_2^{5+}O_7$ systems, respectively. The stability ranges are 1.46 < $R_A/R_B < 1.80$ and $1.4 < R_A/R_B < 2.2$, respectively for the combinations of 3+, 4+ and 2+, 5+ cations (Subramanian et al., 1983). In bismuth-based pyrochlores, the ionic radii of B cations, e.g. niobium, tantalum and antimony are comparable in which they are 0.64 Å for both Nb, Ta and 0.60 Å for Sb under 6 coordination environment. Hence, the weighted R_A/R_B average for both α - $(Bi_{1.5}Zn_{0.5})(Nb_{1.5}Zn_{0.5})O_6O'$ $(Bi_{1.5}Zn_{0.5})(Ta_{1.5}Zn_{0.5})O_6O'$ (BZT) is 1.66 and for $(Bi_{1.5}Zn_{0.5})(Sb_{1.5}Zn_{0.5})O_6O'$ (BZS) is 1.74, which are well within the stability limit for the pyrochlore structure (Mergen et al., 1996; Shannon et al., 1976).

It is worthwhile to highlight that a solid solution is referred as a crystalline phase that can have variable composition. Substitutional solid solutions and interstitial solid solutions are two simple types of solid solutions where the former replaces an atom or homovalent ion in the parent structure and the later involves the introduced species occupies a site that is either empty or no ions/atoms are left out. There are certain prerequisites that must be met to form substitutional solid solutions, i.e. the ions that replace each other must have same charge and similar size. Extensive solid solutions

generally form at high temperatures and the formation of solid solutions at lower temperatures may be more restricted or barely prevailed (West, 1999).

Meanwhile, ions that are substituted by other ions of different charges and additional changes involving creation of vacancies or interstitials (ionic compensation) or electrons or holes (electronic compensation) are known as heterovalent or aliovalent substitution, where these are solid solutions with complex formation mechanism. In addition, two substitutions could take place simultaneously and the substituting ions may be of different charge, providing that overall electroneutrality is preserved (West, 1999).

Practically, solid solution of pyrochlores could be formed by substitution of cations at either A or B site of $A_2B_2O_7$. Inevitably, the substitution may lead to the formation of vacancies, holes or interstitial oxygen that may be related to the interesting electrical properties.

1.6 Problem Statement

Intensive research has been focused on the materials of Bi₂O₃-ZnO-Nb₂O₅/Ta₂O₅ systems due to their interesting dielectric properties. In this project, copper is chosen as the alternative substituent for zinc and investigation of the structural, phase relations and electrical properties of pyrochlores in the Bi₂O₃-CuO-Nb₂O₅/Ta₂O₅ (BCN/BCT) systems is considerably limited. It is important to study the phase compatibilities between binary and/or ternary phases in both systems especially to determine the most appropriate condition for sample preparation. An attempt to enhance the electrical properties of the prepared materials by chemical doping is also part of the investigation. The focus of this study is, therefore, to develop an understanding of the correlation between electrical properties and compositions in these complicated ternary systems.

1.7 Objectives

- 1. To synthesise new pyrochlore phases and to construct the phase diagrams of Bi_2O_3 -CuO- M_2O_5 (M = Nb and Ta) ternary systems using conventional solid state method.
- 2. To identify the phase purities and to investigate the thermal and structural properties of single phase materials using physical and chemical techniques.
- 3. To determine the electrical properties of the prepared samples using ac impedance spectroscopy.
- 4. To enhance the electrical properties and solubility of the pyrochlores through chemical doping.

REFERENCES

- Abe, R., Higashi, M., Sayama, K., Abe, Y. and Sugihara, H. 2006. Photocatalytic activity of R3MO7 and R2Ti2O7 (R=Y, Gd, La; M=Na, Ta) for water splitting into H2 and O2. *The Journal of Physical Chemistry B* 110: 2219-2226.
- Abrahams, I., Krok, F., Struzik, M. and Dygas, J.R. 2008. Defect structure and electrical conductivity in Bi₃TaO₇. *Solid State Ionics* 179: 1013–1017.
- Abram, E.J., Sinclair, D.C. and West, A.R. 2003. A strategy for analysis and modelling of impedance spectroscopy data of electroceramics: Doped lanthanum gallate. *Journal of Electroceramics* 10: 165-177.
- Arenas, D.J., Gasparov, L.V., Qiu, W., Nino, J.C., Patterson, C.H. and Tanner, D.B. 2010. Raman study of phonon modes in bismuth pyrochlores. *Physical Review B* 82: 214302 1-8.
- Bobnar, V., Lunkenheimer, P., Hemberger, J., Loidl, A., Lichtenberg, F. and Mannhart, J. 2002. Dielectric properties and charge transport in the (Sr,La)NbO_{3.5-x} system. Physical Review B 65: 155115.
- Boivin, J.C. and Mairesse G. 1998. Recent Material Developments in Fast Oxide Ion Conductors. *Chemistry of Materials* 10: 2870-2888.
- Brabers, V.A.M. 1969. Infrared spectra of cubic and tetragonal manganese ferrites, *Physica Status Solidi* (b) 33: 563-572.
- Bryntse, I. 1991. Phase analysis and electron microscopy studies of the systems Bi₂O₃-CuO-TiO₂ and Bi₂O₃-CuO-Nb₂O₅. European Journal of Solid State and Inorganic Chemistry 28: 481-492.
- Cai, X., Zhang, L. and Yao, X. 1994. Synthesis and dielectric properties of new compounds with pyrochlore type structure. *Ferroelectrics* 154: 319-324.
- Cann, D.P., Randall, C.A. and Thomas, R.S. 1996. Investigation of the dielectric properties of bismuth pyrochlores. *Solid State Communication* 100: 529-534.
- Chen, A., Yu, Z., Youn, H.J., Randall, C.A., Bhalla, A.S. and Cross, L.E. and Lanagan, M. 2003. Dielectric properties of Bi₂O₃-ZnO-Ta₂O₅ pyrochlore and zirconolite structure ceramics. *Applied Physics Letters* 82: 3734-3736.
- Chen, A., Yu, Z., Youn, H.J., Randall, C.A., Bhalla, A.S. and Cross, L.E., Nino, J. and Lanagan, M. 2002. Low-temperature dielectric relaxation in the pyrochlore (Bi_{3/4}Zn_{1/4})₂(Zn_{1/4}Ta_{3/4})₂O₇ compound. *Applied Physics Letters* 80: 4807-4809.
- Chen, M., Tanner, D.B. and Nino, J.C. 2005. Infrared study of the phonon modes in bismuth pyrochlores. *Physical Review B* 72: 054303 (1-8).
- Chen, S.-Y., Lee, S.-Y. and Lin, Y.-J. 2003. Phase transformation, reaction kinetics and microwave characteristics of Bi₂O₃-ZnO-Nb₂O₅ ceramics. *Journal of the European Ceramic Society* 23: 873-881.

- Cheng, Z.Y., Katiyar, R.S., Yao, X. and Bhalla, A.S. 1998. Temperature dependence of the dielectric constant of relaxor ferroelectrics. *Physical Review B* 57: 8166-8177.
- Choi, G.-K., Kim, D.-W., Cho, S.-Y. and Hong, K.S. 2004. Influence of V₂O₅ substitutions to Bi₂(Zn_{1/3}Nb_{2/3})₂O₇ pyrochlore on sintering temperature and dielectric properties. *Ceramics International* 30: 1187-1190.
- Chon, M.P., Tan, K.B., Khaw, C.C., Zainal, Z., Taufiq Yap, Y.H. and Tan, P.Y. 2012. Synthesis, structural and electrical properties of novel pyrochlores in the Bi₂O₃-CuO-Ta₂O₅ ternary system. *Ceramics International* 38: 4253-4261.
- Christopher, R.S., Licia, M. and Robin, W.G. 2002. Nonstiochiometry in A₂B₂O₇ pyrochlores. *Journal of the American Ceramic Society* 85: 2792-2798.
- Cotton, F.A. and Wilkinson, G. 1972. The Element of the Second and Third Transition Series. In *Advanced Inorganic Chemistry*, pp 923-1076. Canada: John Wiley & Son.
- Du, H., Shi, X. and C, Y. 2010. Defect structure and electrical conduction behaviour of Bi-based pyrochlores. *Solid State Communication* 150: 1213-1216.
- Du, H., Yao, X. and Wang, H. 2006. Dielectric properties of pyrochlore (Bi_{1.5}Zn_{0.5})(Nb_{0.5} M_{1.5})O₇ (M = Ti, Sn, Zr and Ce) dielectrics. *Applied Physics Letters* 88: 212901.
- Du, H. and Yao, X. 2004. Structural trends and dielectric properties of Bi-based pyrochlores. *Journal of Materials Science: Materials in Electronics* 15: 613-616.
- Du, H.L. and Yao, X. 2003. Effects of Sr substitution on dielectric characteristics in Bi_{1.5}ZnNb_{1.5}O₇ ceramics. *Materials Science and Engineering* 99: 437-440.
- Du, H.L. and Yao, X. 2002. Evolution of structure and dielectric properties on bismuth-based pyrochlore with TiO₂ incorporation. *Journal of Electroceramics* 9: 117-124.
- Dyre, J.C. and Schroder, T.B. 2000. Universality of ac conduction in disordered solids. *Reviews of Modern Physics* 72: 873-892.
- Ebbinghaus, S.G. 2007. Influence of composition and thermal treatment on the properties of $Cu_{2+x}Ta_4O_{12+\delta}$. *Progress in Solid State Chemistry* 35: 421–431.
- Felten, E.J. 1967. The preparation of CuNb₂O₆ and CuTa₂O₆. *Journal of Inorganic and Nuclear Chemistry* 29: 1168-1171.
- Fisher, M., Malcherek, T., Bismayer, U., Blaha, P. and Schwarz, K. 2008. Structure and stability of Cd₂Nb₂O₇ and Cd₂Ta₂O₇ explored by *ab initio* calculations. *Physical review B* 78: 014108.
- Fries, T., Lang, G. and Kemmler-Sack, S. 1996. Defect fluorite structures in the Bi-rich part of the system Bi₂O₃□Re₂O₇. *Solid State Ionics* 89: 233-240.
- Funke, K. 1993. Jump relaxation in solid electrolytes. *Progress in Solid State Chemistry* 22: 111-195.

- Granzow, T., Woike, Th., Wohlecke, M., Imlau, M. and Kleemann, W. 2004. Change from 3D-ising to random field-ising-model criticality in a uniaxial relaxor ferroelectric. *Physical Review Letters* 92: 065701 (1-4).
- Grivel, J.-C. 2009. Subsolidus phase relations of the SrO-Ta₂O₅-CuO system at 900°C in air. *Journal of Alloys and Compounds* 486: 293-298.
- Henderson, S.J., Shebanova, O., Hector A.L., McMillan, P.F. and Weller, M.T. 2007. Structural variations in pyrochlore-structured Bi₂Hf₂O₇, Bi₂Ti₂O₇ and Bi₂Hf₂-_xTi_xO₇ solid solutions as a function of composition and temperature by Neutron and X-ray diffraction and Raman spectroscopy. *Chemistry of Materials* 19: 1712-1722.
- Henmi, C.K. 1995. CuBi₂O₄, a new mineral from Fuka, Okayama prefecture, Japan. *Mineralogical Magazine* 59:545-48.
- Herbert, J.M. 1985. Ceramics dielectrics and capacitors, in: D.S. Campbell (Eds.), The Properties of dielectrics, pp. 9. New York: Gordon and Breach.
- Hu, C.Z., Fang, L., Peng, X.Y., Li, C.C., Wu, B. and Liu, L.J. 2010. Dielectric and ferroelectric properties of tungsten bronze ferroelectrics in SrO-Pr₂O₃-TiO₂-Nb₂O₅ system. *Materials Chemistry and Physics* 121: 114-117.
- Irvine, J.T.S., Sinclair, D.C. and West, A.R. 1990. Electroceramics: Characterization by impedance spectroscopy. *Advanced Materials* 2: 132-138.
- Jinling, Y., Jingkui, L., Weihua, T., Ying, S., Xiaolong, C. and Guanghui, R. 1997. Subsolidus phase relations in BiO-GdO-CuO system. *Journal of Alloys and Compounds* 252: 143-147.
- Jonscher, A.K. 1999. Dielectric relaxation in solids. Journal of Physics D: Applied Physics 32: R57-R70.
- Kamba, S., Porokhonskyy, V., Pashkin, A., Bovtun, V., Petzelt, J., Nino, J.C., Trolier-McKinstry, S., Lanagan, M.T. and Randall, C.A. 2002. Anomalous broad dielectric relaxation in Bi_{1.5}Zn_{1.0}Nb_{1.5}O₇ pyrochlore. *Physical Review B* 66: 054106.
- Kennedy, B.J. 1998. Structural trends in pyrochlore-type oxides. *Physica B* 303: 241-243.
- Khaw, C.C., Lee, C.K., Zainal, Z., Miles, G.C. and West, A.R. 2007. Pyrochlore phase formation in the system Bi₂O₃-ZnO-Ta₂O₅. *Journal of the American Ceramic Society* 90: 2900-2904.
- Khaw, C.C., Tan, K.B. and Lee, C.K. 2009. High temperature dielectric properties of cubic bismuth zinc tantalate. *Ceramics International* 35: 1473-1480.
- Khaw, C.C., Tan, K.B., Lee, C.K. and West, A.R. 2012. Phase equilibria and electrical properties of pyrochlore and zirconolite phases in the Bi₂O₃-ZnO-Ta₂O₅ system. *Journal of the European Ceramic Society* 32: 671-680.

- Khaw, C.C., Tan, K.B., Zainal, Z. and Lee, C.K. 2009. Synthesis and characterization of cubic Bi₃Zn₂Ta₃O₁₄ and its related divalent doped pyrochlore materials. Sains Malaysiana 38: 387-393.
- Koops, C.G. 1951. On the dispersion of resistivity and dielectric constant of some semiconductors at audiofrequencies. *Physical Review* 83: 121-124.
- Kumar, M., Rani, S., Bhatnagar, M.C. and Roy, S.C. 2008. Structure, ferroelectric and gas sensing properties of sol–gel derived (Ba,Sr)(Ti,Zr)O₃ thin films. *Materials Chemistry and Physics* 107: 399–403.
- Kwan, C.K. 2004. Electric polarization and relaxation. In *Dielectric Phenomena in Solids*, pp 58-59. Elsevier Inc.
- Leon, C., Rivera, A., Varez, A., Sanz, J., Santamaria, J. and Ngai, K.L. 2001. Origin of constant loss in ionic conductors. Physical Review Letters 86: 1279-1282.
- Levin, I., Amos, T.G., Nino, J.C., Vanderah, T.A., Randall, C.A. and Lanagan, M.T. 2002a. Structural study of an unusual cubic pyrochlore Bi_{1.5}Zn_{0.92}Nb_{1.5}O_{6.92}. *Journal of Solid State Chemistry* 168: 69-75.
- Levin, I., Amos, T.G., Nino, J.C., Vanderah, T.A., Reaney, I.M., Randall C.A. and Lanagan M.T. 2002b. Crystal structure of the compound Bi₂Zn_{2/3}Nb_{4/3}O₇. *Journal of Materials Research* 17:1406-1411.
- Li, B.R. and Mo, Y.H. 1986. Inorganic Dielectric Materials (in Chinese), pp. 360-363. Shanghai Science and Technology Press.
- Li, L., Zhang, X., Ji, L., Ning, P. and Liao, Q. 2012. Dielectric properties and electrical behaviors of tunable Bi_{1.5}MgNb_{1.5}O₇ thin films. *Ceramics International* 38: 3541-3545.
- Li, W. and Schwartz, R.W. 2006. AC conductivity relaxation processes in CaCu₃Ti₄O₁₂ ceramics: grain boundary and domain boundary effects. *Applied Physics Letters* 89: 242906.
- Ling, C.D., Schmid, S., Withers, R.L., Thompson, J.G., Ishizawa, N. and Kishimoto, S. 1999. Solution and refinement of the crystal structure of Bi₇Ta₃O₁₈. *Acta Crystallography* B55: 157-164.
- Ling, C.D., Withers, R.L., Schmid, S. and Thompson, J.G. 1998. A review of bismuth-rich binary oxides in the systems Bi₂O₃-Nb₂O₅, Bi₂O₃-Ta₂O₅, Bi₂O₃-MoO₃, and Bi₂O₃-WO₃. *Journal of Solid State Chemistry* 137:42-61.
- Liu, D.H., Liu, Y., Huang, S.-Q. and Yao, X. 1993. Phase structure and dielectric properties of Bi₂O₃-ZnO-Nb₂O₅-based dielectric ceramics. *Journal of the American Ceramic Society* 76: 2129-2132.
- Liu, Y. and Withers, R.L. 2011. Local structure of relaxor dielectric ceramics, Advances in Ceramics–Electric and Magnetic Ceramics, Bioceramics, Ceramics and Environment, ed. Prof. Costas Sikalidis, pp 87-102. InTech.

- Liu, Y., Withers, R.L., Chen, H., Li, Q. and Tan, H. 2011. Raman spectra, photoluminescence and dielectric relaxation in Bi_{1.5}ZnNb_{1.5}O₇ pyrochlore. *Current Applied Physics* 11: S171-S174.
- Liu, Y., Withers, R.L., Welberry, T.R., Wang, H. and Du, H. 2006. Crystal chemistry on a lattice: The case of BZN and BZN-related pyrochlores. *Journal of Solid State Chemistry* 179: 2141-2149.
- Lufaso, M.W., Vanderah, T.A., Pazos, I.M., Levin, I., Roth, R.S., Nino, J.C., Provenzano, V. and Schenck, P.K. 2006. Phase formation, crystal chemistry and properties in the system Bi₂O₃-Fe₂O₃-Nb₂O₅. *Journal of Solid State Chemistry* 179: 3900-3910.
- Lunkenheimer, P., Fichtl, R., Ebbinghaus, S.G. and Loidl, A. 2004. Non-intrinsic origin of the Colossal Dielectric Constants in CaCu₃Ti₄O₁₂. *Physical Review B* 70: 172102.
- Macdonald, J.R. and Barsoukov, E. 2005. Impedance spectroscopy theory, experiment, and applications, second ed., pp. 9. A John Wiley & Sons, Inc., Publication.
- Mahajan, S., Thakur, O.P., Bhattacharya, D.K. and Sreenivas, K. 2009. Ferroelectric relaxor behavior and impedance spectroscopy of Bi₂O₃ doped barium zirconium titanate ceramics. *Journal of Physics D: Applied Physics* 42: 065413.
- Manning, J.R. 1962. Isotope effect in an electric field and jump frequencies for diffusion in ionic crystals. *Journal of Applied Physics* 33: 2145-2151.
- Masse, J.-P., Szymanowski, H., Zabeida, O., Amassian, A., Klemberg-Sapieha, J.E. and Martinu, L. 2006. Stability and effect of annealing on the optical properties of plasma-deposited Ta₂O₅ and Nb₂O₅ films. *Thin Solid Films* 515: 1674-1682.
- Maxwell, J.C. 1973. Electricity and Magnetism. pp. 88. New York: Oxford University Press.
- McLaren, N.R., Ferrarelli, M.C., Tung, T.W., Sinclair, D.C. and West, A.R. 2011. Synthesis, structure and electrical properties of Cu_{3.21}Ti_{1.16}Nb_{2.63}O₁₂ and the CuO_x-TiO₂-Nb₂O₅ pseudoternary phase diagram. *Journal of Solid State Chemistry* 184:1813-1819.
- Meadowcroft, D.B. 1968. Electronically-conducting refractory ceramic electrodes for open cycle MHD power generation. *Energy Conversion* 8:185.
- Mehraj, S., Ansari, M.S. and Alimddin. 2015. Structural, electrical and magnetic properties of (Fe, Co) co-doped SnO₂ diluted magnetic semiconductor nanostructures. *Physical E* 65: 84-92.
- Mergen, A. and Lee, W.E. 1997. Crystal chemistry, thermal expansion and dielectric properties of (Bi_{1.5}Zn_{0.5})(Sb_{1.5}Zn_{0.5})O₇ pyrochlore. *Materials Research Bulletin* 32: 175-189.

- Mergen, A. and Lee, W.E. 1996. Fabrication and crystal chemistry of Bi_{3/2}ZnSb_{3/2}O₇ pyrochlore. *Journal of the European Ceramic Society* 16: 1041-1050.
- Miles, G.C. and West, A.R. 2006a. Pyrochlore phases in the system ZnO-Bi₂O₃-Sb₂O₅: I. stoichiometries and phase equilibria. *Journal of the American Ceramic Society* 89: 1042-1046.
- Miles, G.C. and West, A.R. 2006b. Pyrochlore phases in the system ZnO-Bi₂O₃-Sb₂O₅: II. Crystal structures of Zn₂Bi_{3.08}Sb_{2.92}O_{14+ δ} and Zn_{2+x}Bi_{2.96-(x-y)}Sb_{3.04-y}O_{14.04+ δ}. Solid State Sciences 8: 1422-1429.
- Natesan, B., Karan, N.K. and Katiyar, R.S. 2006. Ion relaxation dynamics and nearly constant loss behaviour in polymer electrolyte, *Physical Review E* 74: 042801.
- Ngoc, H.N., Petitbon, F. and Fabry, P. 1996. Investigations on the mixed conductivity of copper tantalate. *Solid State Ionics* 92: 183-192.
- Nguyen, B., Liu, Y. and Withers, R.L. 2007. The local crystal chemistry and dielectric properties of the cubic pyrochlore phase in the Bi_2O_3 - $M^{2+}O$ - Nb_2O_5 ($M^{2+}=Ni^{2+}$ and Mg^{2+}) systems. *Journal of Solid State Chemistry* 180: 549-557.
- Nino, J.C., Lanagan, M.T. and Randall, C.A. 2001. Dielectric relaxation in Bi₂O₃-ZnO-Nb₂O₅ cubic pyrochlore. *Journal of Applied Physics* 89: 4512-4516.
- Nino, J.C., Youn, H.J., Michael, T.L. and Randall, C.A. 2002a. Bi₂O₃ solubility of Bi-based pyrochlores and related phases. *Journal of Materials Research* 17: 1178-1182.
- Nino, J.C., Lanagan, M.T., Randall, C.A. and Kamba, S. 2002b. Correlation between infrared phonon modes and dielectric relaxation in Bi₂O₃-ZnO-Nb₂O₅ cubic pyrochlore. *Applied Physics Letters* 81: 4404-4406.
- Nino, J.C., Reaney, I.M., Lanagan, M.T. and Randall C.A. 2002c. Transmission electron microscopy investigation of Bi₂O₃-ZnO-Nb₂O₅ pyrochlore and related phases. *Materials Letters* 57: 414-419.
- Nobre, M.A.L. and Lanfredi, S. 2001. Dielectric properties of Bi₃Zn₂Sb₃O₁₄ ceramics at high temperature. *Materials Letters* 47: 362-366.
- Nobre, M.A.L. and Lanfredi, S. 2002. The effect of temperature on the electric conductivity property of Bi₃Zn₂Sb₃O₁₄ pyrochlore type phase. *Journal of Materials Science: Materials in Electronics* 13: 235-238.
- Nobre, M.A.L. and Lanfredi, S. 2003. Dielectric spectroscopy on Bi₃Zn₂Sb₃O₁₄ ceramic: an approach based on the complex impedance. *Journal of Physics and Chemistry of Solids* 64: 2457-2464.
- Osman, R.A.M. and West, A.R. 2011. Electrical characterization and equivalent circuit analysis of (Bi_{1.5}Zn_{0.5})(Nb_{0.5}Ti_{1.5})O₇ pyrochlore, a relaxor ceramic. *Journal of Applied Physics* 109: 074106-1-8.

- Pannetier, J. and Lucas, J. 1970. New description of the pyrochlore structure Cd₂Nb₂O₆S. *Materials Research Bulletin* 5: 797.
- Panteny, S., Stevens, R. and Brown, C.R. 2005. The frequency dependent permittivity and ac conductivity of random electrical networks. *Ferroelectrics* 319: 199-208.
- Peng, D.S., Shen, B., Zhang, L.Y. and Yao, X. 2004. Study and relationship between sintering atmosphere and dielectric properties for Bi₂O₃-ZnO-Ta₂O₅ system. *Ceramics International* 30: 1199-1202.
- Piir, I.V., Prikhodko, D.A., Ignatchenko, S.V. and Schukariov, A.V. 1997. Preparation and structural investigations of the mixed bismuth niobates containing transition metals. *Solid State Ionics* 101:1141-46.
- Qasrawi, A.F. and Mergen, A. 2012. Structural, electrical and dielectric properties of Bi_{1.5}Zn_{0.92}Nb_{1.5-x}Ta_xO_{6.92} pyrochlore ceramics. *Ceramics International* 38: 581-587.
- Qasrawi, A.F. and Mergen, A. 2010. Energy band gap and dispersive optical parameters in Bi_{1.5}Zn_{0.92}Nb_{1.5}O_{6.92} pyrochlore ceramics. *Journal of Alloy and Compounds* 496: 87-90.
- Rajput, R.K. 2004. A textbook of electrical engineering materials, pp 176-177. Laxmi Publications (P) Ltd.
- Raju, Gorur G. 2003. Polarisation and static dielectric constant. In *Dielectric in Electric Fields*, pp 37-38. New York: Marcel Dekker Inc.
- Rao, P.P., Liji, S.J., Nair, K.R. and Koshy, P. 2004. New pyrochlore-type oxides in Ca-R-Ti-Nb-O system (R = Y, Sm or Gd)-structure, FT-IR spectra and dielectric properties. Materials Letters 58: 1924-1927.
- Ren, W., Susan, T.-M., Randall, C.A. and Thomas, R.S. 2001. Bismuth zinc niobate dielectric thin films for capacitive applications. *Journal of Applied Physics* 89: 767-774.
- Renner, B., Lunkenheimer, P., Schetter, M., Loidl, A., Reller, A. and Ebbinghaus, S.G. 2004. Dielectric behavior of copper tantalum oxide. *Journal of Applied Physics* 96: 4400-4404.
- Roth, R.S. and Waring, J.L. 1962. Phase equilibrium relations in the binary system bismuth sesquioxide-niobium pentoxide. *Journal of Research of the National Bureau of Standards* 66A:451-63.
- Sellami, M., Caignaert, V., Kouadri Hanni, F.Z., Bettahar, N., Benhadria, N, Sari-Mohammed, E., Imine, S. and Bahmani A. 2014. Synthesis and characterisation of new pyrochlore solid solution Bi_{1.5}Sb_{1.5-x}Nb_xCuO₇. *Comptes Rendus Chimie* 17: 899-904.
- Sellami, M., Caignaert, V., Hamdad, M., Bekka, A. and Bettahar N. 2009. Synthesis and characterization of new pyrochlore solid solution Bi_{1.5}Sb_{1.5}Cu_{1-x}Mn_xO₇. *Journal of Alloys and Compounds* 482: 13-18.

- Setter, N. and Waser, R. 2000. Electroceramic materials. Acta Materialia 48: 151-178.
- Shannon, R.D. 1976. Revised effective ionic radii systematic of interatomic distances in halides and chalcogenides. *Acta Crystallographica Section A* 32: 751.
- Shen, B., Yao, X., Kang, L.P. and Peng, D.S. 2004a. Effect of CuO or/and V₂O₅ oxide additives on Bi₂O₃-ZnO-Ta₂O₅ based ceramics. *Ceramics International* 30: 1203-1206.
- Shen, B., Yao, X., Kang, L.P. and Peng, D.S. 2004b. Structure and dielectric properties of Bi₂O₃-ZnO-CaO-Ta₂O₅ ceramics. *Ceramics International* 30: 1-4.
- Silva, S.A. and Zanetti, S.M. 2005. Bismuth zinc niobate pyrochlore Bi_{1.5}ZnNb_{1.5}O₇ from a polymeric urea-containing precursor. *Materials Chemistry and Physics* 93: 521-525.
- Sinclair, D.C., Morrison, F.D. and West, A.R. 2000. Application of combined impedance and electric modulus spectroscopy to characterise electroceramics. *International Ceramics* 2: 33-38.
- Sinclair D.C. and West A.R. 1989. Impedance and modulus spectroscopy of semiconducting BaTiO₃ showing positive temperature coefficient of resistance. *Journal of Applied Physics* 66: 3850-3856.
- Sirotinkin, V.P. and Bush, A.A. 2003. Preparation and dielectric properties of Bi_{1.5}MNb_{1.5}O₇ (M = Cu, Mg, Mn, Ni, Zn) pyrochlore oxides. *Inorganic Materials* 39: 974-977.
- Structural and electrical characteristic of crystalline barium titanate synthesized by low temperature aqueous method. *Journal of Materials Processing Technology* 195: 171-177.
- Struzik, M., Liu, X., Abrahams, I., Krok, F., Malys, M. and Dygas, J.R. 2012. Structure and electrical conductivity in the Bi₂O₃-Ta₂O₅ pseudo-binary system. *Solid State Ionics* 218: 25–30.
- Subramanian, M.A., Aravamudan, G. and Subba Rao, G.V. 1983. Oxide pyrochlores-a review. *Progressive Solid State Chemistry* 15:55-143.
- Szwagierczak, D. and Kulawik, J. 2008. Sintering and dielectric properties of Cu₂Ta₄O₁₂ ceramics. *Journal of the European Ceramic Society* 28: 2075-2083.
- Syed, M., Prasad, G. and Kumar, G.S. 2006. Study of dielectric and impedance relaxations in (Na_{0.125}Bi_{0.125}Ba_{0.65}Ca_{0.1})(Nd_{0.065}Ti_{0.87}Nb_{0.065})O₃ ceramic. Materials Chemistry and Physics 99: 276-283.
- Tan, K.B., Khaw, C.C., Lee, C.K., Zainal, Z., Tan Y.P. and Shaari, H. 2009a. High temperature impedance spectroscopy study of non-stoichiometric bismuth zinc niobate pyrochlore. *Materials Science-Poland* 27: 825-837.

- Tan, K.B., Khaw, C.C., Lee, C.K., Zainal, Z., Tan Y.P. and Shaari, H. 2009b. Phase formation and dielectric properties of pentavalent cation doped non-stoichiometric bismuth zinc niobate (BZN) cubic pyrochlore. Sains Malaysiana 38: 219-226.
- Tan, K.B., Lee, C.K., Zainal, Z., Khaw, C.C., Tan, Y.P. and Shaari, H. 2008. Reaction study and phase formation in Bi₂O₃-ZnO-Nb₂O₅ ternary system. *The Pacific Journal of Science and Technology* 9: 468-479.
- Tan, K.B., Lee, C.K., Zainal, Z., Tan, Y.P. and Shaari, H. 2007. Phase study and electrical properties of divalent doped non-stoichiometric bismuth zinc niobate cubic pyroclore. *Journal of Solid State Science and Technology* 15: 74-81.
- Tan, K.B., Lee, C.K., Zainal, Z., Miles, G.C. and West, A.R. 2005. Stoichiometry and doping mechanism of the cubic pyrochlore phase in the system Bi₂O₃-ZnO-Nb₂O₅. *Journal of Materials Chemistry* 15: 3501-3506.
- Tan, P.Y., Tan, K.B., Khaw, C.C., Zainal, Z., Chen, S.K. and Chon, M.P. 2014. Phase equilibria and dielectric properties of Bi_{3+(5/2)x}Mg_{2-x}Nb_{3-(3/2)x}O_{14-x} cubic pyrochlores. *Ceramics International* 40: 4237-4246.
- Tan, P.Y., Tan, K.B., Khaw, C.C., Zainal, Z., Chen, S.K. and Chon, M.P. 2012. Structural and electrical properties of bismuth magnesium tantalate pyrochlores. *Ceramics International* 38: 5401-5409.
- Ungár, T. 2004. Microstructural parameters from X-ray diffraction peak broadening. *Scripta Materialia* 51: 777-781.
- Valant, M. and Davies, P.K. 2000. Crystal chemistry and dielectric properties of chemically substituted (Bi_{1.5}Zn_{1.0}Nb_{1.5})O₇ and Bi₂(Zn_{2/3}Nb_{4/3})O₇ pyrochlores. *Journal of the American Ceramic Society* 83: 147-153.
- Valant, M. and Suvorov, D. 2005. The Bi₂O₃-Nb₂O₅-NiO phase diagram. *Journal of American Ceramic Society* 88: 2540-2543.
- Valant, M. and Suvorov, D. 2003. Dielectric properties of the fluorite-like Bi₂O₃-Nb₂O₅ solid solution and the tetragonal Bi₃NbO₇. *Journal of the American Ceramic Society* 86: 939-944.
- Vanderah, T.A., Levin, I. and Lufaso, M.W. 2005. An unexpected crystal-chemical principle for the pyrochlore structure. *European Journal of Inorganic Chemistry* 2005: 2895-2901.
- Vanderah, T.A., Lufaso, M.W., Adler, A.U., Levin, I., Nino, J.C., Provenzano, V. and Schenck, P.K. 2006a. Subsolidus phase equilirbria and properties in the system Bi₂O₃:Mn₂O_{3±x}:Nb₂O₅. *Journal of Solid State Chemistry* 179: 3467-3477.
- Vanderah, T.A., Siegrist, T., Lufaso, M.W., Yeager, M.C., Roth, R.S., Nino, J.C. and Yates, S. 2006b. Phase formation and properties in the system Bi₂O₃:2CoO_{1+x}:Nb₂O₅. *European Journal of Inorganic Chemistry* 2006: 4908-4914.

- Van Loan, P.R. 1972. Conductive ternary oxides of ruthenium, and their use in thick film resistor glazes. *American Ceramic Society Bulletin* 51: 231-233.
- Wang, H., Elsebrock, R., Schneller, T., Waser, R. and Yao, X. 2004. Bismuth zinc niobate (Bi_{1.5}ZnNb_{1.5}O₇) ceramics derived from metallo-organic decomposition precursor solution. *Solid State Communications* 132: 481-486.
- Wang, H., Kamba, S., Zhang, M., Yao, X. and Denisov, S. 2006. Microwave and infrared dielectric response of monoclinic bismuth zinc niobate based pyrochlore ceramics with ion substitution in A site. *Journal of Applied Physics* 100: 034109.
- Wang, H., Wang, X. and Yao, X. 1996. Phase transformation and phase distribution of pyrochlore structure in Bi₂O₃-ZnO-Nb₂O₅ system. *Proceedings of 10th IEEE International Symposium on Applications of Ferroelectrics*, East Brunswick, USA, 787–790.
- Wang, H., Wang, X.L. and Yao, X. 1997. Phase equilibrium in Bi₂O₃-ZnO-Nb₂O₅ system. *Ferroelectrics* 195:19-22.
- Wang, H., Yao, X., Zhang, L. and Xia, F. 1999. Phase transition of pyrochlore structure in Bi₂O₃-ZnO-Nb₂O₅ system. *Ferroelectrics* 229: 95-101.
- Wang, H., Zhang, D., Wang, X. and Yao, X. 1998. Effect of La₂O₃ substitutions on structure and dielectric properties of Bi₂O₃-ZnO-Nb₂O₅-based pyrochlore ceramics. *Journal of Materials Research* 14: 546-548.
- Wang, Q., Wang, H. and Yao, X. 2009. Structure, dielectric and optical properties of Bi_{1.5+x}ZnNb_{1.5}O_{7+1.5x} pyrochlores. *Ceramics International* 35: 143-146.
- Wang, Q., Wang, H. and Yao, X. 2007. Structure, dielectric and optical properties of Bi_{1.5}ZnNb_{1.5-x}Ta_xO₇ cubic pyrochlores. *Journal of Applied Physics* 101: 104116.
- West, A.R. 1999. Electrical Properties. In Basic Solid State Chemistry, ed. A.R. West, pp 226-311. New York: John Wiley & Sons, Ltd.
- Wilde, P.J. and Catlow C.R.A. 1998. Defects and diffusion in pyrochlore structured oxides. *Solid State Ionics* 112: 173-183.
- Williamson, G.K.and Hall, W.H. 1953. X-ray line broadening from filed aluminium and wolfram. *Acta Metallurgica* 1: 22-31.
- Withers, R.L., Welberry, T.R., Larsson, A.-K., Liu, Y. Norén, L. Rundlöf, H. and Brink, F.L. 2004. Local crystal chemistry, induced strain and short range order in the cubic pyrochlore (Bi_{1.5-α}Zn_{0.5-β}Nb_{1.5-δ})O(_{7-1.5α-β-γ-2.5δ}) (BZN). *Journal of Solid State Chemistry* 177: 231-244.
- Wu, M.-C., Huang, Y.-C. and Su, W.-F. 2006. Silver cofirable Bi_{1.5}Zn_{0.92}Nb_{1.5}O_{6.92} microwave ceramics containing CuO-based dopants. *Materials Chemistry and Physics* 100: 391-394.

- Yee, K.A., Han, K.R. and Kim, H.T. 1999. The effect of V₂O₅ on the sinterability and physical properties of Bi₂O₃-NiO-Nb₂O₅ and Bi₂O₃-ZnO-Nb₂O₅ temperature-stable dielectrics. *Journal of Materials Science* 34: 4699-4704.
- Youn, H.-J., Randall, C., Chen, A., Shrout, T. and Lanagan, M. T. 2002. Dielectric relaxation and microwave dielectric properties of Bi₂O₃-ZnO-Ta₂O₅ ceramics. *Journal of Materials Research* 17: 1502-1506.
- Youn, H.-J., Sogabe, T., Randall, C.A., Shrout, T.R. and Lanagan, M.T. 2001. Phase relations and dielectric properties in the Bi₂O₃-ZnO-Ta₂O₅ system. *Journal of American Ceramic Society* 84: 2557-2562.
- Zanetti, S.M., Da Silva, S.A. and Thim, G.P. 2004. A chemical route for the synthesis of cubic bismuth zinc niobate pyrochlore nanopowders. *Journal of Solid State Chemistry* 177: 4546-4551.
- Zhang, Y., Zhang, Z.H., Zhu, X.H., Liu, Z.G., Li, Y.Y. and Al-Kassab, T. 2013. Dielectric properties and microstructural characterisation of cubic pyrochlored bismuth magnesium niobates. *Applied Physics A* 115: 661-665.
- Zheng, W.P. 2001. Nanobelts of semiconducting oxides. Science 291: 1947.